New coring study in Augusta Bay expands understanding of offshore tsunami deposits (Eastern Sicily, Italy).

Smedile A.[1*], Molisso F.[2], Chagué C.[3], Iorio M.[2], De Martini P.M.[1], Pinzi S.[1], Collins P.E.F.[4], Sagnotti L.[1], Pantosti D.[1]

1 Istituto Nazionale di Geofisica e Vulcanologia, Roma, Italy

2 Istituto per l'Ambiente Marino e Costiero CNR –IAMC, Napoli, Italy

3 School of Biological, Earth and Environmental Sciences, UNSW, Sydney, Australia

4 Brunel University, London, UK

*Corresponding author: Email: alessandra.smedile@ingv.it

ABSTRACT

Tsunami deposits present an important archive for understanding tsunami histories and dynamics. Most research in this field has focused on onshore preserved remains, while the offshore deposits have received less attention. In 2009 during a coring campaign with the Italian Navy Magnaghi, four 1 m long gravity cores (MG cores) were sampled from the northern part of Augusta Bay, along a transect in 60 to 110 m water depth. These cores were taken in the same area where a core (MS06) was collected in 2007 about 2.3 km offshore Augusta at a water depth of 72 m bsl. Core MS06 consisted of a 6.7 m long sequence that included 12 anomalous intervals interpreted as the primary effect of tsunami backwash waves in the last 4500 years.

In this study, tsunami deposits were identified, based on sedimentology and displaced benthic foraminifera (as for core MS06) reinforced by X-ray fluorescence data. Two erosional surfaces (L1 and L2) were recognized coupled with grain size increase, abundant *Posidonia oceanica* seagrass remains and a significant amount of *Nubecularia lucifuga,* an epiphytic sessile benthic foraminifera considered

to be transported from the inner shelf. The occurrence of Ti/Ca and Ti/Sr increments, coinciding with peaks in organic matter (Mo inc/coh) suggests terrestrial run-off coupled with an input of organic matter. The L1 and L2 horizons were attributed to two distinct historical tsunamis (AD 1542 and AD 1693) by indirect age-estimation methods using ^{210}Pb profiles and the comparison of Volume Magnetic Susceptibility data between MG and MS06 cores. One most recent bioturbated horizon (Bh), despite not matching the above listed interpretative features, recorded an important paleoenvironmental change that may correspond to the AD 1908 tsunami. These findings reinforce the value of offshore sediment records as an underutilized resource for the identification of past tsunamis.

Keywords: Eastern Sicily, offshore coring, tsunami, sedimentology, foraminifera, XRF core scanning

INTRODUCTION

Onshore tsunami sedimentary signatures are generally well studied and their recognition in the geological record is widespread. In the last two decades, several authors (e.g., Dawson and Stewart, 2007; Kortekaas and Dawson, 2007; Morton *et al.*, 2007; Shiki *et al.*, 2008; Chagué-Goff *et al.*, 2011; Goff *et al.*, 2012) have proposed criteria to recognize onshore historic and paleotsunami deposits based primarily on the identification of sedimentary structures, the recognition of geochemical and geomorphological imprints as well as the detection of changes in the paleontological content (Mamo *et al.*, 2009; Pilarczyk *et al.*, 2014). On the other hand, offshore deposits and their sedimentary fingerprint in the geological record, although considered to offer a higher potential in terms of preservation and spatial coverage (Rhodes *et al*., 2006; Dawson and Stewart, 2007; Goff *et al.*, 2012), remain less known and explored. After the 2004 Indian Ocean and 2011 Tohoku-oki tsunamis, offshore surveys were conducted to collect material, mainly from the inner continental shelf (0-30 m below sea

level (bsl)) and over the shelf-break (> 100 m bsl). These studies highlighted that in the marine realm the tsunami-related units are subjected to the action of currents, waves and bioturbation that occur immediately after their deposition (Feldens *et al.*, 2012; Sakuna *et al.*, 2012; Ikehara *et al.*, 2014; Tamura *et al.*, 2015; Yosigawa *et al.*, 2015; Seike *et al.*, 2017). Thus, it is often not easy to recognize offshore tsunami deposits even when they are related to recent events or with a precise age control (Toyofuku *et al.*, 2014) because of their potentially low preservation in shallow water due to reworking and transport by currents, waves (Weiss and Bahlburg, 2006) and gravity flows which disperse sediment on the continental shelves. Moreover, differentiation of tsunami layers from other distinguishable units associated to flash-floods or major storms may be problematic (Milker *et al.*, 2013). Therefore, nearly the whole published research emphasizes the importance of local conditions (geology, coastal and offshore bathymetry/topography, sedimentation regime, vegetation, etc.) and it is regularly noted that no single indicator serves as a stand-alone proxy to identify tsunami-laid sediments (Chagué-Goff *et al.*, 2011; Goff *et al.*, 2012; Sakuna *et al.*, 2012; Shanmugan, 2012). Offshore evidence of paleotsunamis has been sparsely studied compared with the onshore record (Abrantes *et al.*, 2008; Goodman-Tchernov *et al.*, 2009; Paris *et al.*, 2010; Sakuna *et al.*, 2012; Smedile *et al.*, 2012; Goodman-Tchernov *et al.*, 2016; Quintela *et al.*, 2016; Tyuleneva *et al.*, 2018), and a unique toolkit for the identification of offshore tsunami deposits has not been defined yet. In fact, approaching offshore analysis as any other environmental analysis requires much attention, and a multitude of approaches and proxies to identify and characterize tsunami deposits is needed (e.g. shallow geophysics, sedimentological and textural, micropaleontological, geochemical features).

The study presented here focuses on a range of analyses carried out on newly collected cores (MG) along an E-W transect from 60 to 110 m bsl to identify sediment transport patterns associated with tsunami backwash along the Augusta Bay shelf (Eastern Sicily, Italy) (Fig. 1).

Another objective is to determine through correlation the lateral presence of the shallow horizons identified in a 6.7 m-long piston-core (MS06), collected in the same area in 2007, at 72 m bsl. Results obtained from core MS06 highlighted 12 anomalous intervals, marked by peaks with a high percentage of displaced epiphytic foraminifera (taxa that are normally living in the infralittoral zone on vegetated and coarse substrates such as the seagrass *Posidonia oceanica*) and sandy component increments, which were interpreted as the primary effect of tsunami backwash waves (Smedile *et al.*, 2011). Altogether these objectives can contribute to better tsunami hazard assessment of an important coastal area with historically documented tsunami occurrence (AD 1169, AD 1693 and AD 1908) and onshore evidence for tsunami deposits associated with historical and pre-historical events (De Martini *et al.*, 2010; 2012).

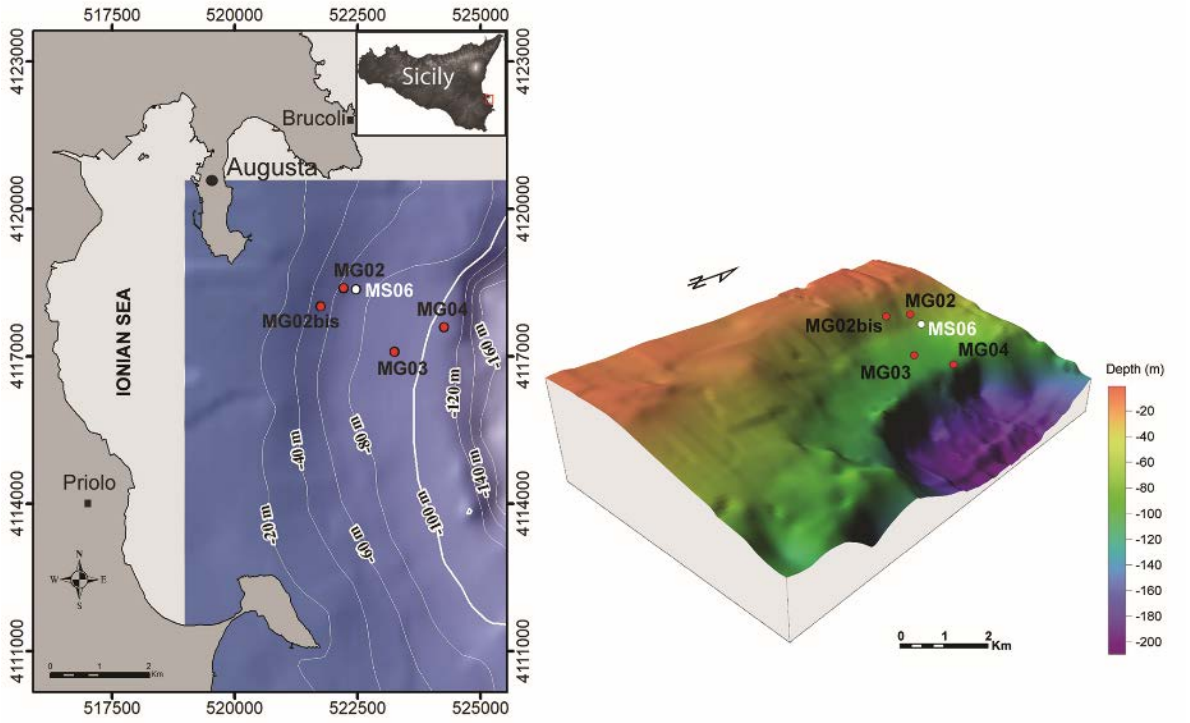

Figure 1 Map (on the left) of Augusta Bay area modified from Smedile *et al.* (2011) and compiled using bathymetric contours (spacing 20 m) enhancing the topography; on the right a DEM (modified after Pirrotta *et al*., 2013) showing the seafloor morpho-bathymetry after the LGM. In both the location of cores MG (red dots) discussed in this study and of core MS06 (white dot) are shown. The location study site is also shown in a geographic map of Sicily in the inset on the upper right.

STUDY SITE

Augusta Bay in SE Sicily is a wide gulf facing the Ionian Sea (Fig. 1) characterized in the NW sector by the seasonal outflows of the Mulinello, Marcellino and Cantera small streams which drain mainly Mesozoic-Quaternary carbonatic derived sediments (ISPRA, 2011). Streams outflows are generally poor and with very localized hydrodynamic effects (Lisi *et al*., 2009) as demonstrated by the recognition of recent foraminiferal assemblages referring to freshwater contributions localized only very close to the stream mouths in the NW sector of the Bay (Romano *et al.*, 2013). This area was affected by at least three historical tsunamis (AD 1169, AD 1693 and AD 1908), whose deposits were identified and characterized onshore (Schicchitano *et al.*, 2007; Barbano *et al.*, 2010; De Martini *et al.*, 2010; Schicchitano *et al.*, 2010). Because of positive onshore tsunami evidence, Augusta Bay was chosen for offshore coring (MS06 core) in 2007 to search for any subtle sediment anomalies, such as fauna assemblage, physical properties, grain size etc., that could provide evidence for tsunami occurrence in the offshore record (Smedile *et al.*, 2011). Within that study a geophysical survey was carried out in the bay with seismic reflection chirp-sonar profiles covering 150 km^2, which allowed us to compile a bathymetric/seafloor- reflectivity map and better understand the stratigraphy of the collected core (Smedile *et al.*, 2011; Pirrotta *et al.*, 2013). Furthermore, the bathymetry of Augusta Bay is characterized by a narrow continental shelf and a relatively steep slope (from 2 to 4%) up to approximately 5 km from the present shoreline, with the shelf edge ranging between 120 and 140 m bsl (Fig. 1). The northern part of the bay exhibits a wider shelf and fine-grained lithology and the absence of features possibly related to large erosive/re-depositional processes caused by the effects of currents or slumps, thus representing the ideal location to sample MS06, a CP-20 piston core, 6.7 m long, collected by the CNR R/V *Urania* at 72 m bsl, about 2 km offshore (Smedile *et al.*, 2011). A first age model for the sedimentary

sequence of core MS06 was based on radiocarbon dating, tephrochronology and short-lived radionuclide ratios (Smedile *et al.*, 2011). The age model was then further refined by high-resolution paleomagnetic and rock magnetic data, which provided original high-resolution geomagnetic paleosecular variation (PSV) and relative paleointensity (RPI) curves spanning the last 4 ka (Sagnotti *et al.*, 2011). Two geological and geophysical parallel studies, performed in the offshore area of Augusta Bay (Firetto Carlino *et al.*, 2013; Pirrotta *et al.*, 2013), pointed out active tectonic processes during the Holocene supporting the hypothesis of a connection between the offshore area and the active tectonics structures responsible for the historical regional seismicity and tsunamis (e.g. the two strongest events in AD 1169 and AD 1693).

Besides its importance for tsunami and seismic hazard studies, Augusta Bay is also a site of national interest due to its high environmental pollution risk. Indeed, the harbor has experienced serviced industrial plants and commercial activities for over half a century, including many petroleum and petrochemical plants. As a consequence, a wide range of contaminants (Hg, Pb, Cu, heavy hydrocarbons, etc.) have been introduced into the harbor since the early 1960s, and have been partially retained in the sediments (Romano *et al.*, 2009; Sprovieri *et al.*, 2011; Bellucci *et al.*, 2012; Croudace *et al.,* 2015) due to the contemporary construction of outer breakwaters. The high pollution levels in Augusta Bay (especially for Hg), have presumably caused stressful conditions to *Posidonia oceanica*, leading to its complete disappearance as detailed in several studies (Di Leonardo *et al*., 2007, 2008; 2009; Sprovieri *et al.*, 2011). The seagrass *P. oceanica* is a long-lived endemic species of the Mediterranean Sea, which generates monospecific meadows along the coast at water depths between 1 and 40 m bsl, the latter being actually marked by an irregular and patchy distribution dead mat in the Augusta Bay area (Di Leonardo *et al.*, 2017). The original environment was also modified over time by sediment dredging within the port and its relative settlement in both legal and illegal disposal offshore

areas (Bellucci *et al.*, 2012). Thus, much of the literature is also focused on the effects of industrial activity and its relative contaminant influence on the coastal ecosystem as a whole (Decembrini *et al*., 2004; Raffa and Hopkins, 2004) and especially on the living benthic foraminiferal communities based on data from shallow cores and box-core stations within the harbor (Romano *et al.*, 2013; 2015; Bergamin *et al.*, 2016; Romano *et al.,* 2018) and from the outer shelf in the southern part of Augusta Bay (Di Leonardo *et al.*, 2007).

MATERIAL AND METHODS

Sampling

In June 2009 during a campaign with the Italian Navy Ammiraglio Magnaghi, four 1 m long gravity cores (hereafter MG cores), were collected from the northern part of Augusta Bay, along a transect 60 to 110 m bsl, near the location of the previously collected core MS06 (Fig. 1; Table 1). The MG cores were sampled using a SW-104 corer, patented by CNR-IGM, designed to preserve an optimal sediment−water interface and to obtain a section of sediment up to 1.2 m in length with minimized coring disturbance (Magagnoli and Mengoli, 2000). The sampling strategy was designed based on previously acquired seismic data and bottom reflectivity. Particular attention was paid to avoid dredged and dumping areas and therefore a Van-Veen grab was used to test each sampling site prior to coring.

Table 1 – Cores location

Core	Latititude	Longitude	Depth m bsl	Length (cm)
MG02bis	37°12'30.00"N	15°14'42.00"E	-60 m	110
MG02	37°12'41.98"N	15°15'0.97"E	-64 m	103
MG03	37°12'0.00"N	15°15'42.98"E	-93 m	118
MG04	37°12'15.98"N	15°16'23.99"E	-108 m	93

Laboratory analyses

All collected cores (MG02bis, MG02, MG03 and MG04) were stored in the refrigeration cell at the IAMC-CNR core repository in Naples and, in 2010 were split length-wise, measured, photographed, described at cm-scale, and later sub-sampled for further analyses. Since one of the main goals was to apply the same multidisciplinary approach as for MS06 core, except for X-ray imaging, the same laboratory analyses (petrophysical, ITRAX X-ray fluorescence (XRF), grain size and micropaleontological) were performed on all MG cores. Radiocarbon and short lived radionuclide (^{210}Pb and ^{137}Cs) dating was carried out on two selected cores, MG02bis and MG04. based on the availability of adequate ^{14}C material as well as the need to choose two cores for short lived radionuclide representative of the mid-inner and outer shelf (MG02bis and MG04).

Physical properties were measured at 1 cm intervals on the archive half of the cores, 1 h after the core was split, using a fully automated GEOTEK Multi-Sensor Core Logger (MSCL) at the IAMC-CNR Physical Properties Laboratory. The MSCL system includes a Bartington MS2E Point sensor to measure the low-field volume magnetic susceptibility (VMS), with a spatial resolution of 0.4 cm. Values were log plotted, visually compared in order to detect similar trends, and according to their physical properties, correlate to the lithological layering.

From each MG core, u-channel holders were sub-sampled for XRF scanning and stored before analysis at the EMCOL Core Analysis Laboratory at Istanbul Technical University. U-channels were then analyzed using an ITRAX XRF core scanner equipped with a molybdenum X-ray source set to 30 kV, 50 mA, an exposure time of 10 s, and steps of 1 mm. Up to 34 elements were determined and recorded as counts per second (cps), although only results of elements of interest are presented here. Counts were normalized over cps to correct for grain size and variations in surface geometry (e.g. Croudace and Rothwell, 2015), while the ratio of incoherent over coherent scattering (Mo Inc/Mo Coh: Mo ratio) is

used as a proxy for organic content (e.g. Chagué-Goff *et al.,* 2016). Normalized data and Mo Inc/Mo Coh (Mo ratio) were also processed using R software for principal component analysis (PCA).

Sedimentological and micropaleontological analyses were conducted at the CNR-IAMC in Naples and INGV in Rome, respectively. Samples were collected with a variable spacing from 1 cm to 10-12 cm with a denser sampling in coarse grained intervals or where sedimentary structures and peculiar enrichment layers of the *P. oceanica* seagrass remnants were observed in order to characterize any peculiar change in the studied sequences. The description of textural constituents was based on microscope observations of dried-sieved sand (>30 µm). Grain-size distribution was determined using sieves with mesh sized spaced at one-phi interval between -3 ϕ and +4 ϕ and a Helos/KF/Quixel Sympatec laser analyzer for the fraction <63 mm. Samples for micropaleontological analysis were washed and passed through 63 µm (230 mesh) and 125 µm (120 mesh) sieves, oven-dried at 40°C, and divided into equal aliquots using a microsplitter. Counting was performed on subsamples of approximately 300 benthic foraminifera specimens only on the fraction >125 µm to avoid juvenile specimens, while the 63-125 µm fraction was preserved for future research. Planktonic foraminifera were also simultaneously counted and identified. For each sample the P/B ratio (P = number of planktonic foraminifera and B = number of benthic foraminifera) was also calculated, because it is normally assumed to be correlated to increasing bathymetry depth (Van der Zwaan *et al.*, 1990). Benthic foraminiferal genera were classified following Loeblich and Tappan (1987) and foraminiferal species were identified following previous studies on Mediterranean benthic taxa (Cimerman and Langer, 1991; Sgarrella and Moncharmont Zei, 1993; Fiorini and Vaiani, 2001) and finally interpreted following Jorissen (1987), Sgarrella and Moncharmont Zei (1993) and Murray (2006). Images of selected benthic species were acquired using a JEOL (JSM-6500F) thermal field emission scanning microscope (FESEM). Benthic foraminiferal density (BFN) was calculated as the number of specimens per gram of dry sediment (specimens/g) according to

Scott et *al.* (2001). Following the same procedure (specimens/g), the epifauna vs infauna ratio was calculated, among the most abundant and common species (i.e. >4% in at least one sample), by grouping taxa and using ecological preference listed in Murray (2006). A two-way (Q-mode and R-mode) Hierarchical Cluster Analysis (HCA) was applied on a matrix with relative abundance of commonly occurring species (i.e.>4% in at least one sample) by means of the Ward's linkage method, using the software package PAleontological STatistics (PAST, version 2.17c; Hammer *et al.*, 2001). This technique was applied to identify groups of samples with similar faunal content and to recognize their characterizing species (Parker and Arnold, 1999).

Chronology

Three well-preserved *Nucula* sp. bivalve shells were collected from cores MG02bis and MG04 for Accelerator Mass Spectrometry (AMS) radiocarbon dating that was carried out at Poznan Radiocarbon Laboratory (Poland) and Beta Analytic Radiocarbon Dating Laboratory (Florida, USA). Radiocarbon ages were calibrated using MARINE13 Calibration curve (Reimer *et al.*, 2013).

^{210}Pb and ^{137}Cs activities were measured for the uppermost 20 cm of MG02bis and MG04 cores at the IRNS-LAME laboratories (France) via gamma spectrometry. This method permits the simultaneous measurement of ^{214}Pb (a daughter isotope of ^{226}Ra) and hence determination of the *in situ* or 'background' ^{210}Pb, and the atmospheric ^{210}Pb ($^{210}Pb_{excess}$) (Appleby, 2001). Prior to analysis, samples were dried at 40°C, *P. oceanica* seagrass remnants removed, weighed, and ground to powder. ^{210}Pb age estimates were determined using the Constant Rate of Supply model (CRS) (Goldberg, 1963; Appleby, 2001), where the ages reflect the vertical profile of $^{210}Pb_{excess}$ and its known decay rate (half-life = 22.3 yr). The fairly uniform reduction in $^{210}P_{excess}$ with depth suggests the ^{210}Pb signal is dominated by the atmospheric flux (Appleby, 2001) and hence the CRS model can be applied. The variability in ^{226}Ra

suggests some variability of *in situ* ^{210}Pb production, and there are some relatively small changes in sediment type, so the apparent precision of calculated age estimates may be overly optimistic. While age estimates up to 150 years are theoretically possible, 100-120 years are a more realistic maximum as it becomes increasingly difficult to differentiate $^{210}Pb_{excess}$ from the background production (Cundy and Croudace, 1996).

^{137}Cs in the samples is derived from artificial sources (Appleby, 2001), with global dispersal and deposition being recorded in sediments from AD 1953-1954 (about 10 years after the start of atmospheric nuclear testing), and deposition reaching a maximum in AD 1963 (Nuclear Test Ban Treaty) and AD 1986 (Chernobyl nuclear accident), the latter event being recorded only in some areas in the northern Hemisphere. Previous investigations in Augusta Bay (Cundy *et al.*, 1998; Collins *et al.*, 2001) found a clear *circa* AD 1963 ^{137}Cs peak, but no AD 1986 peak, possibly reflecting wind directions at the time.

Correlations of VMS trends with those obtained for core MS06 and acquired in 2007 at the IAMC-CNR, as well as ^{210}Pb derived age constraints, provide the chronostratigraphic control of the MG stratigraphic sequence.

RESULTS

Core sedimentology and Volume Magnetic Susceptibility analyses

Sedimentological analysis of MG cores indicates that the sequence is dominated by bioturbated clayey silt with interbedded layers and lenses rich in bioclasts (Figs. 2 and 3). Based on sedimentological analysis three main lithofacies associations can be recognized, from bottom to top:

Facies A: Homogeneous, olive grey mud, made of clayey silt with rare, thin lenses of sandy silt, where the sandy fraction is mostly constituted by *P. oceanica* remains and reworked bioclasts (bivalves, gastropods and bryozoan fragments, sometimes abraded and/or bioeroded).

Facies B: Sandy silt and clayey silt with diffused silty sand lenses. This facies directly overlies Facies A and consists of two normally graded units (L1 and L2 in Figs 2 and 3) with sharp erosional contacts. The two units are represented by medium-fine to fine-very fine sand, with abundant, non-reworked bioclast fragments (mollusk shells, bryozoans) and *P. oceanica* remains and are characterized by sand lenses commonly concentrated at the unit bottom. At the base of L1 in core MG02bis, soft mud pebbles, likely derive from erosion and reworking of the underlying sediments (Facies A), have been found in association with rare, well rounded, flat pebble stones with average size of 1.5 cm.

Facies C: Bioturbated sandy clayey silt. This unit is characterized by an increase of the sandy fraction towards the top of the cored sequence and overall normal grading. A 5-11 cm thick, bioturbated dark gray horizon (Bh, in Figs 2 and 3), rich in organic material, was sampled by all MG cores at 10-25 cm depth beneath the seafloor (bsf).

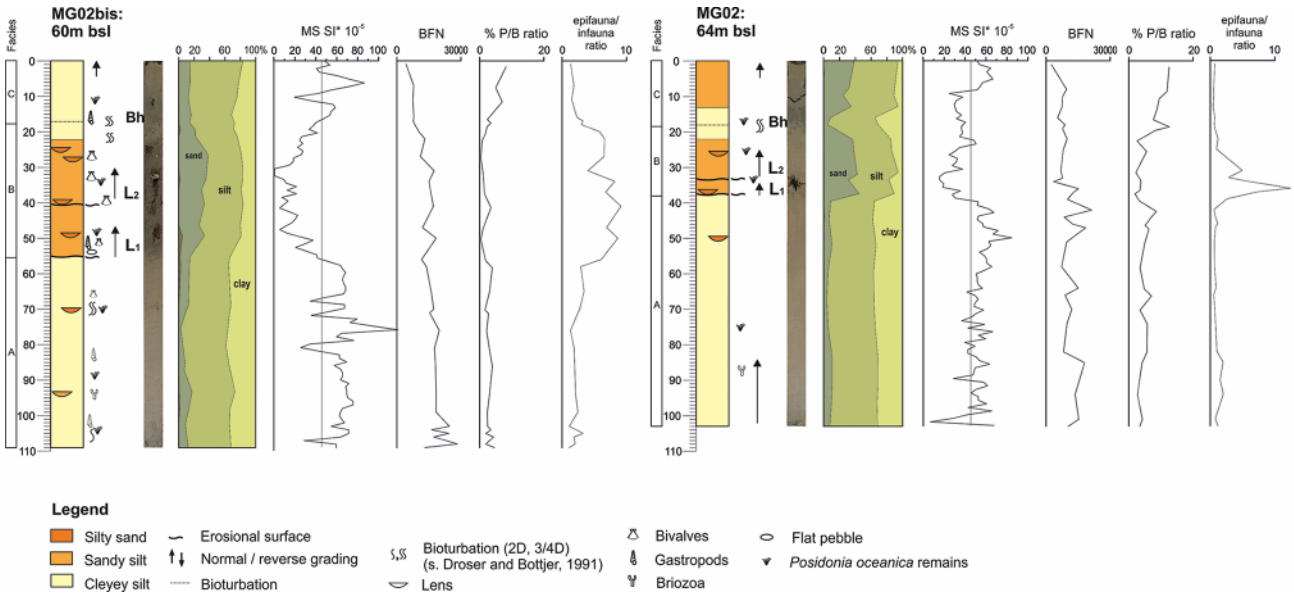

Figure 2 Lithology, textures, sedimentary structures, core photo and VMS plot of cores MG02bis and MG02. On the left of the lithological columns the three facies associations recognized within the cored succession are displayed. L1, L2 and Bh refer to the main units identified in core stratigraphy. Down core distribution of the benthic foraminiferal density (BFN) calculated as specimens/g, P/B ratio and the epifauna vs infauna ratio are reported.

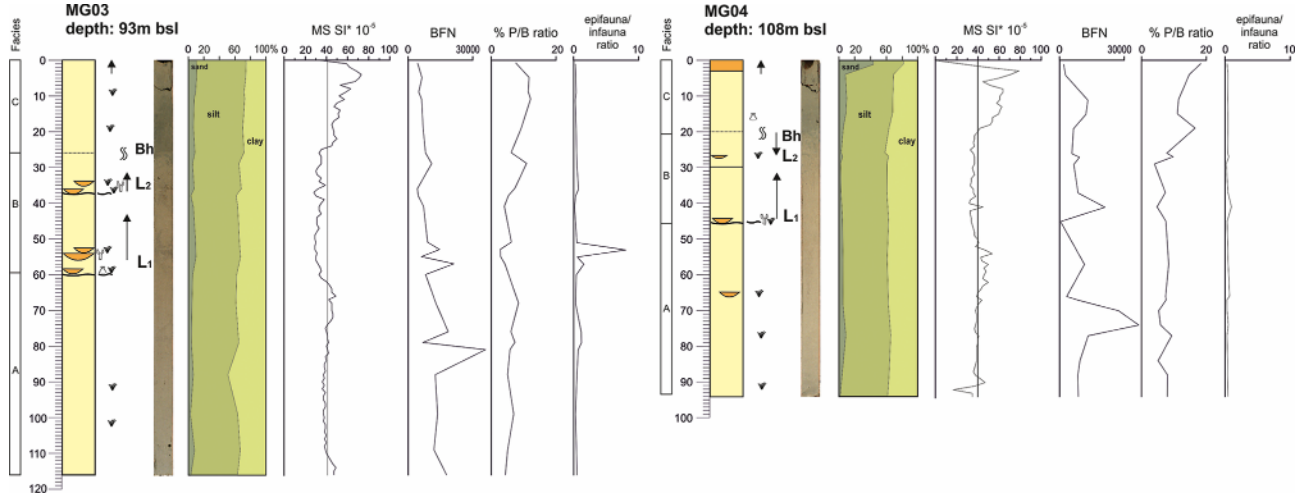

Figure 3 Lithology, textures, sedimentary structures, core photo and VMS plot of cores MG03 and MG04. On the left of the lithological columns the three facies associations recognized within the cored succession are displayed. L1, L2 and Bh refer to the main units identified in core stratigraphy. Down core distribution of the benthic foraminiferal density (BFN) calculated as specimens/g, P/B ratio and the epifauna vs infauna ratio are reported. For legend see also Fig. 2.

Among all MG VMS data set (Figs. 2 and 3), mean values, standard deviation and data trends were analyzed. VMS data showed a good agreement with grain size variations. The average and the patterns of VMS profiles are similar for cores in pairs, likely due to the same depositional setting within the continental shelf (e.g. the average is 45.83±24.2, 47.60± 14.5 and 40.9±9.2, 40.5±9.8 SI x 10^{-5} for MG02bis, MG02 and MG03, MG04, respectively). Cores MG02bis and MG02 (Fig. 2) display two large VMS wavering patterns in their upper portion, and then higher and more stable values in the older part of the sequence, with several distinct peaks (the highest up to 118 SI x 10^{-5} in MG02bis). On the other hand, cores MG03 and MG04 show fairly constant VMS values, with the exception of two intervals exhibiting relatively higher values (between 0-25 and 0-20 cm bsf and 60-75 and 52-65 cm bsf in MG03

and MG04, respectively) (Fig. 3). The mean value, standard deviation and trends were also analyzed for the uppermost 1 m bsf of core MS06 (unpublished data), using the same sensor and methodology to that for the MG cores. MS06 display a mean value of 48.6±6.9 SI x 10^{-05} with a VMS trend fairly constant around that mean value except for the 30-43 cm bsf interval, where relatively higher values up to 70 SI x10^{-05} occur.

Benthic foraminifera

Benthic foraminifera were found in all collected samples and results are expressed as relative abundances (counts and photos of selected species in Table S1 and Fig. S2, respectively); most of them are always rare, with percentage lower than 4%, or were only found in a few samples. In cores MG02bis and MG02 (31 samples analyzed), 236 benthic foraminifera species pertaining to 95 genera and 213 benthic species belonging to 95 genera were recognized, respectively. In core MG03, a total of 23 samples were analyzed and 183 benthic species pertaining to 84 genera were identified. Similarly, in MG04 146 benthic foraminifera species belonging to 78 genera were identified in 20 samples. Foraminiferal density, represented as BFN in Figs. 2 and 3, shows a general constant decrease from the bottom to the top in all MG cores and almost high frequency fluctuating trends enhanced in correspondence of the Facies B or its bottom. Moreover, the latter peculiar trend characterizes few samples in MG03 and MG04 (Fig. 3) with very low BFN where the entirely picked washed residue, contained a low number of foraminiferal specimens (less than 150 and 100 in MG03 and MG04, respectively). On the other hand, planktonic foraminifera are present in limited amounts and their assemblage principally consists of *Globigerina* spp. and *Globigerinoides* spp. (Table S1). In the P/B ratio a fairly constant value is found from the bottom to the top with a clear increase in the topmost 20 cm bsf (Figs. 2 and 3). It is interesting to note that Facies B is commonly characterized by low P/B ratio.

Furthermore, P/B ratio shows mean values of 2.8%, 5.6%, 6.9% and 8.9%, moving from the shallow to the deeper cores.

As for the relative abundance, in cores MG02bis and MG02 the dominant species is *Nubecularia lucifuga* with percentages of up to 38% and 22%, respectively. Furthermore, in MG02bis common taxa are also *Ammonia* spp. (13%), *Miliolinella* spp. (13%) and *Rosalina* spp. (12%). In MG02, *N. lucifuga* is followed by *Ammonia* spp. (16%), *Nonionoides turgidus* (15%) and *Elphidium advenum* and *Valvulineria bradyana* to a lesser extent. Conversely, the MG03 core is dominated by *Ammonia* spp. (26%) and *V. bradyana* (18%) with *Cassidulina carinata*, *E. advenum*, *Nonion communae* and *N. turgidus* as subsidiary species (up to 12-15%). In MG04, the abundant species *V. bradyana* (21%) and *Ammonia* spp. (20%) are accompanied by *C. carinata* (18%), *N. turgidus* (17%) and *E. advenum* (16%).

Miliolinella spp., *N. lucifuga* and *Rosalina* spp. are epifaunal taxa generally living on plants or sediments as part of the phytal assemblage living on seaweeds and seagrasses of the inner shelf (Murray 2006). The genus *Ammonia* includes infaunal forms that tolerate low-oxygen concentration and a wide range of salinity, is often associated with riverine discharge or a brackish environment (Sen Gupta, 1999; Murray, 2006). *E. advenum*, *N. communae*, *N. turgidus* and *V. bradyana* are infaunal species, related to muddy substratum rich in nutrients and organic detritus (Jorissen, 1987; Murray, 2006). The species *C. carinata* can exhibit both an infaunal and epifaunal behavior (Murray, 2006) and is considered typical of muddy bottoms (Sgarrella and Moncharmont *Ze*y, 1993).

Taking into account the above mentioned characteristics the epifauna/infauna ratio was calculated and usually ranged between 0 and 1 along all the MG cores (Figs. 2 and 3). Clear peaks of the latter ratio can be noted in correspondence with Facies B (up to 9, 13 and 8 in MG02bis MG02 and MG03, respectively) while within the fairly flat low trend of MG04 only a peak value of 0.9 is detectable.

Table 2 – Alphabetical list of the benthic foraminifera taxa exceeding 4% of relative abundance in at least one sample and used in HCA.

List of taxa used in the statistical analysis	MG02bis	MG02	MG03	MG04
Ammonia spp.	X	X	X	X
Asterigerinata mamilla (Williamson)	X		X	
Bulimina marginata d'Orbigny		X	X	X
Cassidulina carinata Silvestri	X	X	X	X
Discammina compressa (Goëss)		X		
Elphidium aculeatum (d'Orbigny)	X			
Elphidium advenum (Cushman)	X	X	X	X
Elphidium crispum (Linnaeus)		X		
Gavellinopsis spp.	X	X	X	
Globocassidulina subglobosa (Brady)			X	X
Lobatula lobatula (Walker and Jacob)		X		
Massilina gualteriana (d'Orbigny)	X	X		
Melonis barleeanum (Williamson)		X		
Miliolinella spp.	X	X	X	X
Neocorbina posidonicola (Colom)	X			
Nonion commune (d'Orbigny)		X	X	
Nonionoides turgidus (Williamson)	X	X	X	X
Nubecularia lucifuga Defrance	X	X	X	X
Peneroplis pertusus (Forskal)	X			
Porosononium granosum (d'Orbigny)	X			
Quinqueloculina spp.	X	X	X	X
Rectuvigerina phlegeri Le Calvez		X		X
Rosalina spp.	X	X	X	X
Sigmoilina costata Schlumberger	X	X	X	X
Valvulineria bradyana (Fornasini)	X	X	X	X

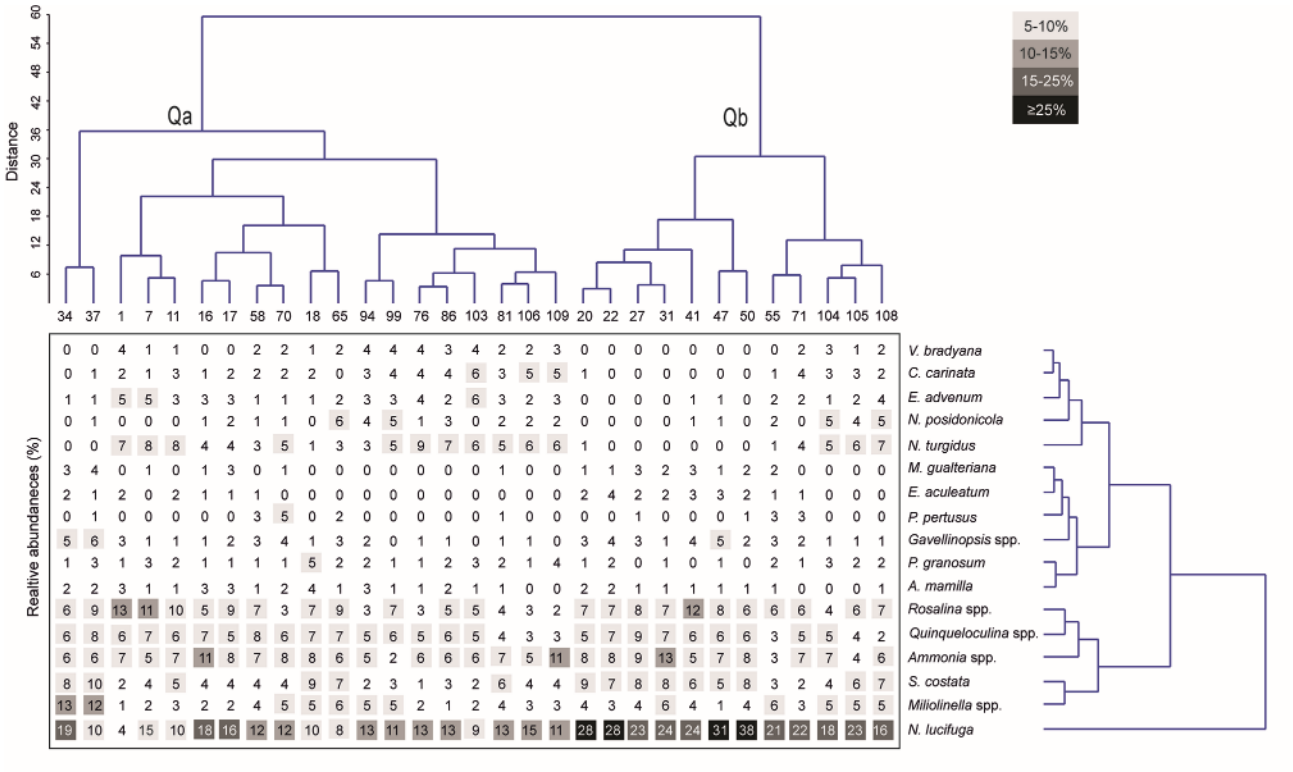

Figure 4 Core MG02bis two-way cluster analyses using Ward-linkage, based on the relative abundance of species. Relative abundances (>4%) of species are categorized using fixed range values.

Since each MG core shows differences in terms of percentage of single species and distribution along the sequence, the applied HCA revealed similar grouping in all cores (see Table 2 for a list of those taxa used for HCA). For this reason, the two way HCA is shown for MG02bis (Fig. 4, while MG02, MG03 and MG04 HCA are in Figs. S3, S4 and S5) and synthesized for all MG cores in Table 3 where foraminiferal assemblage characterizing each cluster was labeled with the name of the most representative and abundant species together with data related to the dominant and accompanying species in each cluster.

Table 3 – MG cores foraminiferal assemblages (dominant and accompanying species) characteristic for each cluster (Q- mode HCA). The dominant facies recognizable for each cluster is also reported. In parenthesis the abundance value for each species among the samples pertaining to the same cluster is displayed.

Core	Facies	Cluster	Assemblage	Dominant taxa	Accompanying taxa
MG02bis	A/C	Qa	*N. lucifuga /Miliolinella* spp. assemblage	*N. lucifuga* (19%) *Miliolinella* spp. (13%)	*Ammonia* spp. (11%) *Rosalina* spp. (11%)
	B	Qb	*N. lucifuga* assemblage	*N. lucifuga* (38%)	*Ammonia* spp. (13%), *Rosalina* spp. (12%) *Quinqueloculina* spp. (9%) *S. costata* (9%)
MG02	B	Qa	N. *lucifuga* assemblage	*N. lucifuga* (22%)	*Miliolinella* spp. (12%) *Quinqueloculina* spp. (9%) *S. costata* (9%) *Rosalina* spp. (9%)
	A	Qb	*Ammonia* spp. assemblage	*Ammonia* spp. (16%)	*N. lucifuga* (11%) *N. turgidus* (11%) *V. bradyana* (9%)
	C	Qc	*Ammonia* spp. /*N. turgidus* assemblage	*Ammonia* spp. (15%) *N. turgidus* (15%)	*E. advenum* (10%) *V. bradyana* (10%) *C. carinata* (8%) *R. phlegeri* (7%)
MG03	B	Qa	N. *lucifuga* assemblage	*N. lucifuga* (22%)	*N. turgidus* (13%) *V. bradyana* (13%) *Ammonia* spp. (12%)
	C	Qb	*Ammonia* spp. assemblage	*Ammonia* spp. (26%)	*C. carinata* (15%) *E. advenum* (15%) *N. communae* (14%)
	A	Qc	*Ammonia* spp. /*V. bradyana* assemblage	Ammonia spp. (22%) *V. bradyana* (18%)	*E. advenum* (13%) *C. carinata* (13%) *N. turgidus* (9%) *B. marginata* (8%)
MG04	C	Qa	*C. carinata* /*N. turgidus* assemblage	*C. carinata* (18%) *N. turgidus* (17%)	*Ammonia* spp. (16%) *E. advenum* (15%) V*. bradyana* (11%)
	A	Qb	*V. bradyana*/*Ammonia* spp. assemblage	*V. bradyana* (21%) *Ammonia* spp. (20%)	*E. advenum* (16%) *C. carinata* (15%) *B. marginata* (11%)
	B	Qc	*Ammonia* spp. /*V. bradyana* assemblage	*Ammonia* spp. (18%) *V. bradyana* (17%)	*E. advenum* (15%) *N. lucifuga* (13%) *B. marginata* (10%)

The MG02bis two-way HCA, carried out on 17 species and groups of taxa (Table 2), divided the analyzed samples into clusters Qa and Qb (Q mode in Fig. 4). Cluster Qa lumped samples from 0-19 cm bsf (whole Facies C), two samples that encircle the depth interval within 34-37 cm bsf (Facies B) and most of the analyzed samples are from 57-109 cm bsf (whole Facies A). The cluster Qa is dominated by *N. lucifuga* (19%) and *Miliolinella* spp. (13%) along with the accompanying species *Ammonia* spp. (11%), *Rosalina* spp. (11%) and *N. turgidus* (9%). The cluster Qb (*N. lucifuga* assemblage) grouped samples in the depth interval 20-55 cm bsf (whole Facies B) along with two other shorter intervals, at 71 cm bsf and at the bottom core (Facies A). Samples of cluster Qb are characterized by high percentage of the dominant species *N. lucifuga* (16-38%), and the accompanying taxa, *Ammonia* spp. (13%), *Rosalina* spp. (12%), *Quinqueloculina* spp. (9%) and *Sigmoilina costata* (9%). Similarly, the performed HCA on the others MG cores showed that samples can be grouped into three clusters mostly linked to the three main identified sedimentological facies (Table 3).

Geochemistry

In core MG02bis, the silty clay sequence below units L1 and L2 exhibits high counts of Si, K, Fe, Mn, Rb Zn and Zr, but low Mo ratio (low organic matter) associated with low counts of Ca, S, Cl and Br, all displaying little vertical variation. A similar trend was observed in the Bh layer, while the top gray layer has high Br counts increasing upward, but also high Si, K and Rb counts (Figs. 5 and S6). The L1 and L2 units (22-55 cm bsf in MG02bis) on the other hand are characterized by four organic-rich intervals, as shown by peaks in Mo ratio that are also coincident with peaks in Br (Fig. 5). These units are also marked by lower counts of a number of elements, namely Si, K, Rb, Mn, Fe and Zn, linked to a lower magnetic susceptibility, but increased pulses of Ti/Ca and Ti/Sr ratios that generally match the higher organic matter (Figs. 5 and S6). It is however interesting to note that the base of unit L1 displays sharp maximum

peaks in Si, K, Fe, Mn, Zr and Sr immediately below the peak in organic matter, probably representing the deposition of inorganic material, unless this is the result of the sum-closed effect sometimes reported in studies using ITRAX core scanners (e.g. Löwemark *et al.*, 2011). PCA shows that just over 55% of the variance can be explained by the first two components, PC1 (34.8%) and PC2 (20.5%). In PC1, Cl, Br and S plot close to Mo ratio, thereby reflecting their strong association with organic matter, while detrital elements plot on the other side, representing the mineralogy of the sediments. In PC2, there are two groups, namely Ti/Ca and Ti/Sr exhibiting a strong positive loading, while Sr and Ca display a strong negative loading (Fig. 5). A similar pattern is observed in MG02 and MG03 cores (Figs. S7, S8), although the signatures are more subtle.

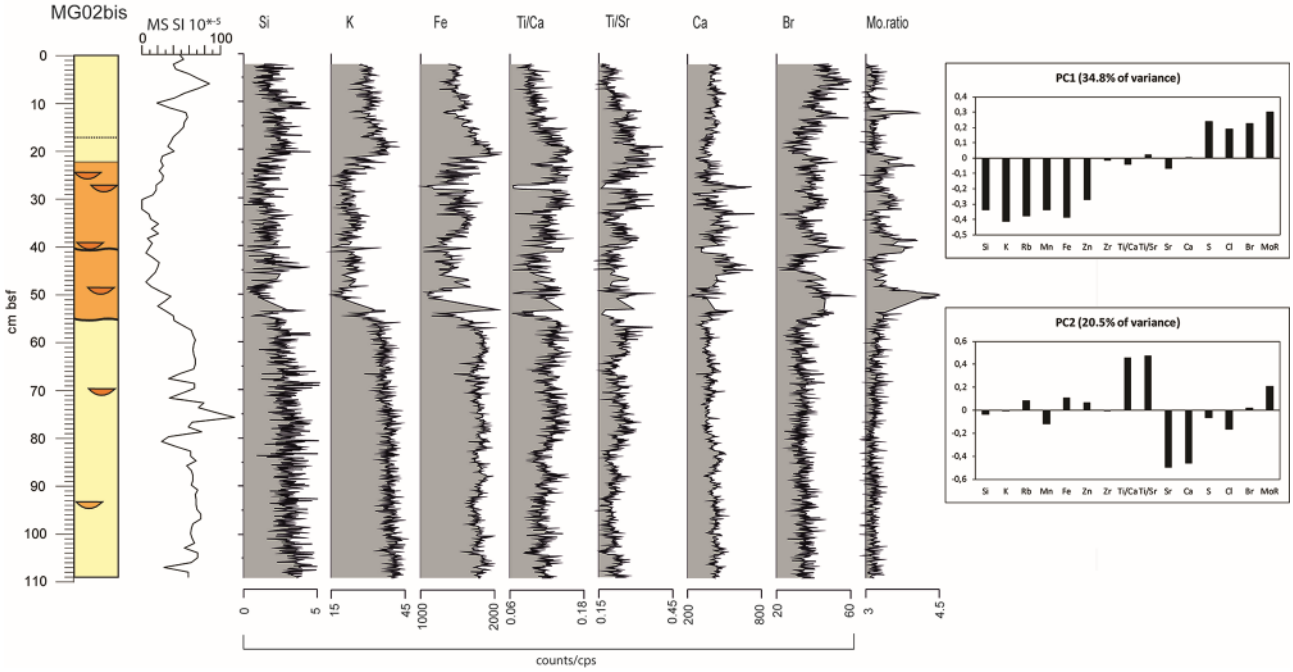

Figure 5 MG02bis stratigraphy, volume magnetic susceptibility, selected ITRAX counts (normalized over cps), Mo ratio (a proxy for organic matter). On the right eigenvalues for each element and MoR (=Mo ratio) for the 1st principal component (PC1) and the 2nd principal component (PC2); the percentage of variance for PC1 and PC2 is also shown.

Short lived radionuclides and radiocarbon

The ^{210}Pb age estimate profiles to a depth of 20 cm in cores MG04 and MG02bis (Fig. 6) show a progressive increase in age with depth, with a disturbance at around 10 cm depth in both cores. In core MG04 (Fig. 6B), sediments at 20 cm depth date to around AD 1900- 1910, while sediments at the same depth in MG02bis (Fig. 6A) may be slightly older, although the age model shows greater uncertainty. Sediment accumulation rates at both core sites have varied over time (Fig. 6C). Low rates at the base of the MGS02bis profile appear to represent an artefact of low $^{210}Pb_{excess}$ values and the dating model. Both cores show a progressive increase in accumulation rate towards the mid-20th Century, with MG02bis peaking at around AD 1960, while MG04 peaked between ca. AD 1960-1965, with the slight difference possibly reflecting local variability. Both cores then show a reduction in sedimentation rates back towards pre-disturbance values, before increasing again from around AD 1980 until 2009.

The ^{137}Cs profiles for MG04 and MG02bis fluctuate around 5 bq kg^{-1} in most samples and therefore were deemed inconclusive. The lower activity levels in the lowest two samples for MG02bis probably reflect the maximum limit of downwards migration of ^{137}Cs in pore water (e.g. Wang *et al.*, 2015).

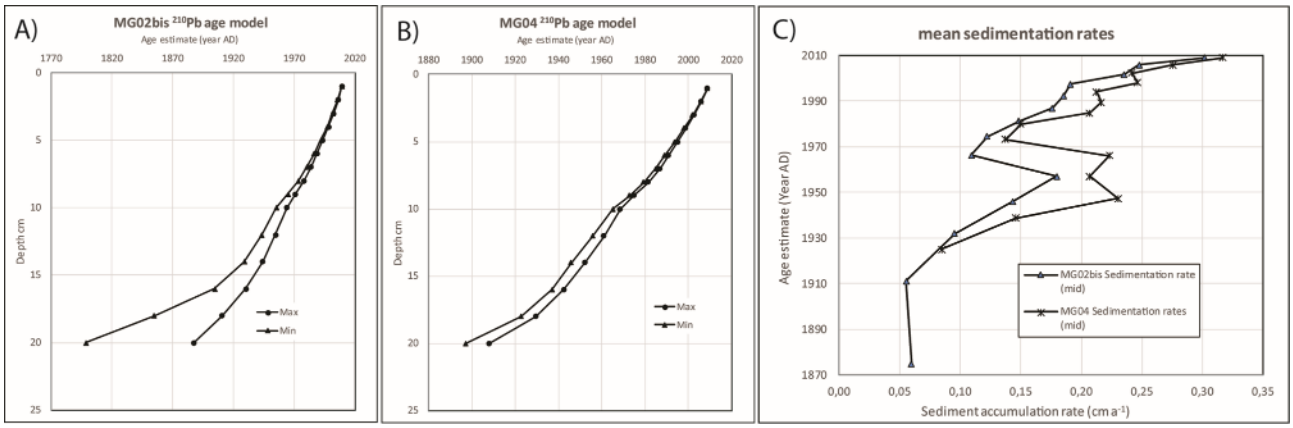

Figure 6 ^{210}Pb activity with depth for cores MG02bis (A) and MG04 (B); age depth curves (C) based on ^{210}Pb chronology showing the mean sedimentation rate for the topmost 20 cm in both cores.

Results of radiocarbon dating performed only on three *Nucula* sp. shells are shown in Table 4. No more reliable dating material (e.g. shells, vegetal remains), in terms of weight quantity, preservation state and position within the stratigraphic sequence was found in cores MG, apart those found in L1 and L2 units that were considered potentially displaced and or reworked. Moreover, it was decided to not date both *Turritella* specimens found in core MG02bis due to their mobility behavior within sediments nor *P. oceanica* remnants and organic matter rich layers because of the high level of pollution of the study area (Budillon *et al*., 2008). Despite this preventive caution, ^{14}C dating did not yield trustworthy results; in fact all ages were too young (or invalid adding the ΔR=124±30 to the calibration), taking into account their stratigraphic position and the ^{210}Pb and ^{147}Cs data collected from the same cores.

Table 4 - Results from AMS dating and calibrations using the MARINE13 curve

Sample code	Lab code	depth (m)	δ C^{13}	Measured Age BP	Cal AD/BC ranges	
MG02bis-83	Poz-41245	0.83	+3.8	470±30	1725	1950*
MG02bis-102	Poz-41244	1.02	+2.1	525±30	1693	1950*
MG04-77	Beta-298	0.77	+0.8	400±30	invalid age	

DISCUSSION

Based on sedimentological analysis, three main lithofacies are recognized in the MG cores dominated by clayey silt deposits with interbedded lenses and layers rich of bioclasts. In particular, the intermediate Facies B showed two sandy intervals (L1 and L2), characterized by sharp basal contact, bioclasts abundance and well preserved *P. oceanica* remains. Furthermore, a bioturbated horizon (Bh) in Facies C marked the onset of a dark grey interval ranging 5-11 cm in thickness, rich in organic material, characterizing the most recent sediments in the MG cores.

Analytical results from MG cores confirmed strong similarities between the two cores located within the inner-mid shelf (MG02bis and MG02, 60 and 64 m bsl, respectively) as well as between those two

sampled next to the shelf edge (MG03 and MG04, 93 and 108 m bsl, respectively). Differences between core pairs can be interpreted as the result of their position with respect to the morpho-bathymetry of the northern part of Augusta Bay. In fact, as shown in Figure 1, the proximal part of the shelf presents terraced surfaces bounded by steep escarpments seawards, with these outer edges roughly following the coast. Such surfaces deepen to about 80 m bsl and are deeply incised by straight erosional cuts, outlining a well-developed relict superficial drainage system related to the LGM as reported by Firetto Carlino *et al.* (2013). In this morpho-bathymetric setting, MG02bis and MG02 cores, that are collected at the base of the outer edge of these marine terraces and next to such incised erosional cuts, show large variability in terms of grain size, sedimentary structures as well as in the content of fossils and *P. oceanica* remains, compared to the two cores near the shelf edge (MG03 and MG04) dominated by almost constant finer grained sediments. Besides their inherent differences, all MG cores can be correlated due to the occurrence of the two distinct units (L1 and L2) potentially associated with high energy events based on the following (Fig. 7). Both L1 and L2 units show a normal grading and are characterized by shell debris, well preserved whole shells and abundant fresh *P. oceanica* remains differently from the sandy silt lenses belonging to the Facies A. In the stratigraphy of all MG cores the erosional base of L1 and L2 units represents a strong signature that can be traced up to the shelf break (Fig. 7). In MG02bis the coarse grained deposit visible at 22-55 cm bsf resulted thicker, very rich in shell content and *P.* oceanica remains respect to the same interval visible in core MG02 where the two units are thinner and contain a lower shell content. Towards the outer shelf, in MG03 and MG04 cores, the sandy silt facies of L1 and L2 are replaced by a clayey silt with sandy silt lenses just above their basal erosional surfaces. Despite grain size differences, the presence of abundant *P. oceanica* remains as well as whole shells together with a clear grading likely support the correlation of L1 and L2 along the shelf

profile reinforcing their interpretation as two different high energy events at basin scale and thus favoring a tsunami back wash origin instead of storms and slumps.

As already discussed by Quintela *et al.* (2016), a strong textural signature (sand-sized unit) is highly unlikely at ca. 100 m depth bsl similar to what was observed in offshore shallow areas of Sendai Bay after the 2011 Tohoku-oki tsunami. There, grain size analysis suggested that the offshore transport of coarse sand by backwash was of limited extent, mainly due to the gentle shelf morphology (Tamura *et al.*, 2015).

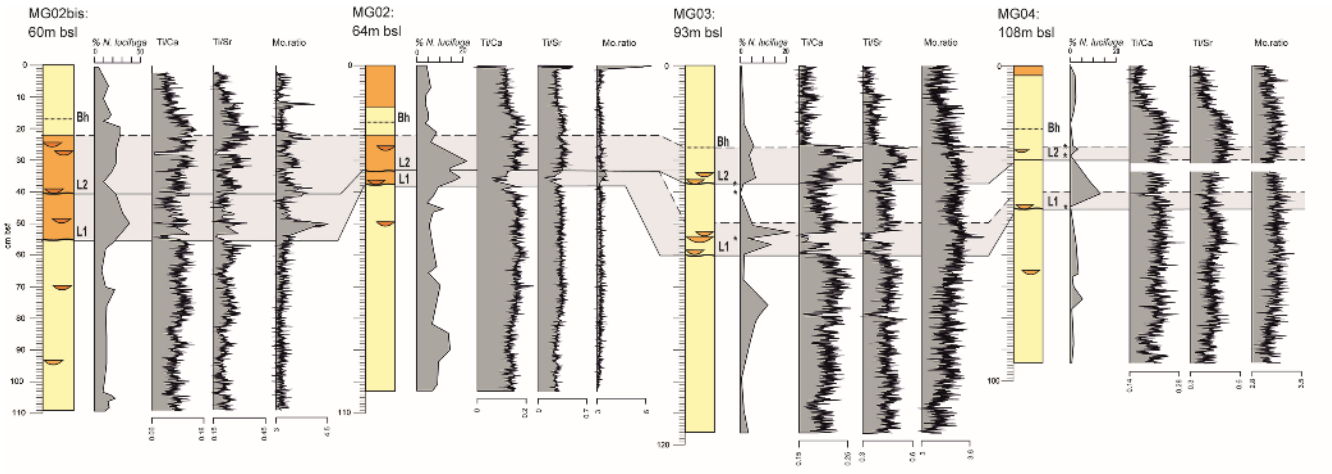

Figure 7 – Cross core MG correlation showing stratigraphy, *N. lucifuga* trend, elemental ratio (Ti/Ca and Ti/Rb) and Mo ratio. Asterisks next to *N. lucifuga* distribution graph mark samples with low foraminifera tests in cores MG03 and MG04 (less than 150 and 100, respectively). Shaded areas cover the hypothesized thickness of units L1 and L2 obtained matching evidence interpreted as related to transport of material from shallower to deeper depth along shelf (sedimentological and micropaleontological evidence) and run-off from the land (XRF results).

Units L1 and L2 can be interpreted as tsunami deposits also by matching sedimentological data with benthic foraminifera content and selected XRF parameters (Fig. 7). Cores MG02bis and MG02 displayed a benthic foraminifera assemblage, mostly related to the coarseness of the substratum and vegetation, as testified by the presence of many epiphytic foraminifera taxa (e.g *Ammonia* spp., *N. lucifuga*, *Quinqueloculina* spp., *Rosalina* spp., *S. costata*, etc.). Moreover, the common recovery of *N. turgidus*

and *V. bradyana* suggests a muddy substratum rich in organic matter consistent with intermediate depths (mid-outer shelf), as highlighted in cores MG03 and MG04 and in lesser extent in MG02. Notably, the often irregular distribution of cluster assemblages along the study sequence (Table 3) point out that benthic foraminifera are sometimes affected by significant transport, likely due to bottom currents (Raffa and Hopkins, 2004), as highlighted by the widespread distribution of *Ammonia* spp. from the mid-inner to the outer shelf. In fact, *Ammonia* spp. that is normally assumed to live in muddy sand substrates of brackish lagoons and of the inner-shelf (Sgarrella and Moncharmont Zei, 1993; Murray 2006), showed unusually higher percentages in MG03 and MG04 with respect to MG02bis and MG02. Moreover, the frequent recovery of yellow and oxidized *Ammonia* tests in most of the picked samples did not allow to use this taxon to recognize a different provenance (brackish vs marine). On the other hand, specimens pertaining to *N. lucifuga* (i.e. the dominant assemblage species found in most samples collected comprising L1 and L2) showed well preserved tests, often still attached to *P. oceanica* fibers coinciding with the samples collected within Facies B (Photos in S2). In all MG cores, HCA pointed out that, beyond the different cluster assemblages, *N. lucifuga* can represent an allochthonous element of selected intervals. It is well known that *N. lucifuga* is an epiphytic sessile species (Langer, 1993), with a flat shape, living for its entire one-year long life permanently attached to its substrate that can be made by sand grains or larger plants (i.e. phanerogams) (Mateu-Vincens *et al.*, 2012; 2014). Based on the analyzed samples, *N. lucifuga*, although quite variable in percentages, displayed different average distribution values along the shelf profile (10-15% in MG02bis, 5-10% in MG02 and < 5% in MG03 and MG04). These differences can be interpreted as the effect of dead species dispersal by bottom currents or during storms likely responsible for the patchy recovering of *P. oceanica* remains together with *N. lucifuga* and epiphytic foraminifera as observed in the lenses in Facies A and described by Murray (2006) as floating plants phenomenon. On the contrary, greater values are displayed by the allochthonous

taxon especially in units L1 and L2 (up to 38% in MG02bis, 22% in MG02, 21% in MG03 and 13% in MG04) (Fig. 7), thus showing differences between the inner-mid shelf and the outer-shelf distribution of coarse sediments. Indeed, the occurrence of *N. lucifuga* is also related to coarse grains distribution on the shelves, as discussed above. A positive relationship can be displayed between *N. lucifuga* distribution and a corresponding increase in BFN values and the epifauna/infauna ratio as shown within the L1 and L2 units (Figs. 2 and 3). In particular, the epifauna/infauna ratio highlights how the statistical 'isolation' of *N. lucifuga* cannot be considered as a reflection of its general dominance but is a result of an overall increase of faunal density linked to an increased input of epifaunal taxa commonly present in the inner shelf at shallow depth. Moreover, in MG03 and MG04 six samples (asterisks in Fig. 7) collected within and at the base of L1 and L2, did not contain enough foraminifera specimens to be considered statistically representative of the study sample as confirmed by very low values in BFN. Indeed, this reduction of foraminifera can be interpreted as related to a major input of fine sediments, as also observed elsewhere in modern offshore tsunami samples collected close to shelf-break (Ikehara *et al.*, 2014; Tamura *et al.*, 2015).

The occurrence of displaced benthic foraminifera and their interpretation in terms of submarine sediment transport and deposition by backwash waves have already been discussed by many authors who studied 2004 and 2011 tsunami deposits (Sugawara *et al.*, 2009; Jonathan *et al.*, 2012; Milker *et al.*, 2013; Toyofoku *et al.*, 2014) as well as the 1755 historical tsunami deposit off the Algarve coast in Portugal (Quintela *et al.*, 2016). Hence, it was observed that in several offshore tsunami layers, displaced foraminifera species along with backwash coarse grained sediments are often represented by a significant amount of coastal foraminifera (marine/estuarine species as well as epiphytic taxa) often combined with organic matter enrichment. Preservation of foraminiferal test (i.e. patterns of fragmentation, abrasion and corrosion) and specimen's size in anomalous horizons, were also described

as characteristic of the tsunami deposits left by the 2011 Tohoku-oki tsunami (Pilarczyk *et al*., 2012) or as possible indicator of onshore paleotsunami events (Pilarczyk and Reinhardt, 2012; Pilarczyk *et al*., 2014). Nevertheless, they were evaluated as indicative of a paleoenvironmental change.

The elemental distribution in the MG cores (Fig. 5 and Fig. S6), except for units L1 and L2 (Fig. 7), is in line with that reported for the uncontaminated sediments of inner Augusta Bay, which consist primarily of carbonates (Ca, Sr) and clays (Si, K, Rb) (Croudace *et al.*, 2015) as well as the outcropping geology, dominated by carbonates and volcanoclastics/volcanics within muddy sediments and calcarenites (Grasso and Lentini, 1982). While the Ca and Sr signatures dominate the marine sediment, due to the occurrence of carbonates (e.g. Chagué-Goff *et al.*, 2017), Ti/Ca and Ti/Sr most likely reflect the terrigenous input, with Ti sourced from volcanics, gneiss and schists and thus often used as indicator of terrestrial material in onshore or offshore tsunami deposits (e.g. Chagué-Goff *et al.*, 2017). Titanium has also been recorded in offshore sediments as a result of increased rainfall and associated runoff (e.g. Yarincik *et al.*, 2000; Haug *et al.*, 2001), and has also been used as a provenance marker (e.g. Stuut *et al.*, 2007). An increase of Ti/Ca was reported by Sakuna *et al.* (2012) as characterizing a backwash deposit of the 2004 Indian Ocean Tsunami offshore Pakarang Cape, Thailand, and a similar interpretation can be used here, even if the geology is different; carbonates dominate the marine sediments, while Ti is more prevalent in terrestrial sediments. In core MG02bis (Fig. 7), the L1 and L2 units are characterized by a marked coarsening of sediment, and Ti/Ca and Ti/Sr peaks, coinciding with peaks in organic matter (Mo ratio), suggesting run-off from the land coupled with an input of organic matter. Unit L1 seems to be characterized by a single pulse of terrestrial material, while in L2 two to three different pulses are observed, as suggested by the relative increase of the Mo ratio, which might represent successive backwash waves. In core MG02, a change in organic matter and terrestrial input

is also visible in units L1 and L2 even if clear peak values highlighting different pulses are not as evident. In cores MG03 and MG04, a subtle increase in Ti/Ca and Ti/Sr overlies a layer at the base of L1 with high Ca, Sr and organic matter. In layer L2, there is a small peak overlain by a large peak suggesting terrestrial run-off in MG03, while in MG04 there is only a subtle change in Ti/Ca and Ti/Sr ratios.

In addition, results shown in Figure 7, pointed out the difficulty to trace the topmost limit of the L1 and L2 events. In cores MG03 and MG04 the L1 unit apparently displays an increased thickness similar to that shown in MG02bis and MG02 where the top boundary limit is overlain by the erosional surface of L2. Nevertheless, combined results in Figure 7 suggest a decrease in thickness of L1 in MG03 and MG04 due to the fact that the micropaleontological and geochemical evidence is confined to the lowermost part of the L1 unit and thus suggests a physical separation with the L2 event. As for the L1, the topmost limit of the L2 unit cannot be well defined especially due to its proximity to the Bh horizon as shown in MG03. Moreover, in core MG03, the Bh horizon deepens and becomes thicker likely mixing up sediments in between Bh and L2.

The complexity of drawing the topmost limit of L1 and L2 events might be explained with the fact that tsunami deposits can be modified or removed by subsequent physical (Shinozaki *et al.*, 2015; Tamura *et al.*, 2015) and/or biological processes (Seike *et al.*, 2016). Indeed, after the 2011 tsunami some offshore stations were monitored, revealing that the recolonization by benthic organisms began within several months after the event (Seike *et al.*, 2013), and post-depositional biogenic alteration continued over much longer time scales (Seike *et al.*, 2016) concealing the topmost limit of the Tohoku-oki deposit (Seike *et al.*, 2017). Furthermore, even if the Bh horizon represents an important stratigraphic signature recognizable all along the shelf (Fig. 2), the analysis did not yield suitable information to support an origin as related to a high energy event as suggested for units L1 and L2 (Fig. 7). Nevertheless, in a

speculative reasoning, it could be argued that this peculiar layer could represent a marked paleoenvironmental change in the most recent stratigraphy.

MG cores ages and correlation with MS06 core

Results presented in Figure 7 show that, thanks to the combination of sedimentological, micropaleontological and geochemical data, it is possible to collect valuable information about backwash dynamics in the offshore sedimentary record of past tsunamis. However, key questions arise concerning the possibilities that the identified L1 and L2 units repersent a single high energy event with several pulses as shown by cores MG02bis and MG02 or as well as two distinct events close in time as probably displayed in cores MG03 and MG04.

No clear evidence to strongly support one or the other of the two hypotheses, especially because of the marked erosive character of L2 that concealed the topmost limit of unit L1 in the two shallower cores.

Uncertainties related to radiocarbon dating did not lead to a refined age model for all MG cores and only some ages derived from ^{210}Pb profiles retrieved from cores MG02bis and MG04 (Fig. 6) can be added to the MG stratigraphy. Nevertheless, a correlation among all four cores can be established, comparing the VMS trends, only for the upper portion of cores (reaching a maximum depth of 80 cm in MG02bis). In this interval, five increasing/decreasing VMS trends and three VMS marker peaks, correlating with grain size results, were identified. In detail, peak 1 is related to a sandy-mud interval while peaks 2 and 3 identify an increase in the clay fraction (Figs. 2, 3 and 8). Moreover, the correlation of MG data to VMS data of core MS06 provided some indirect age constraints to the MG stratigraphic sequence. In Figure 8 the correlation of the VMS trends show that the MG cores correlate with the uppermost 50 cm of MS06. Moreover, the MG cores collected the topmost 8-10 cm (trend I) that were

lost in core MS06. Such a correlation allows us to transfer ^{14}C dating, carried out on core MS06 (Smedile *et al.*, 2011) to cores MG, which, coupled with ^{210}Pb activities, contributes to the construction of an events time scale. On this basis, peaks 2 and 3 could be considered younger than 1000 B.P. as they occur immediately before the ^{14}C age obtained for MS06 (AD 885-1200).

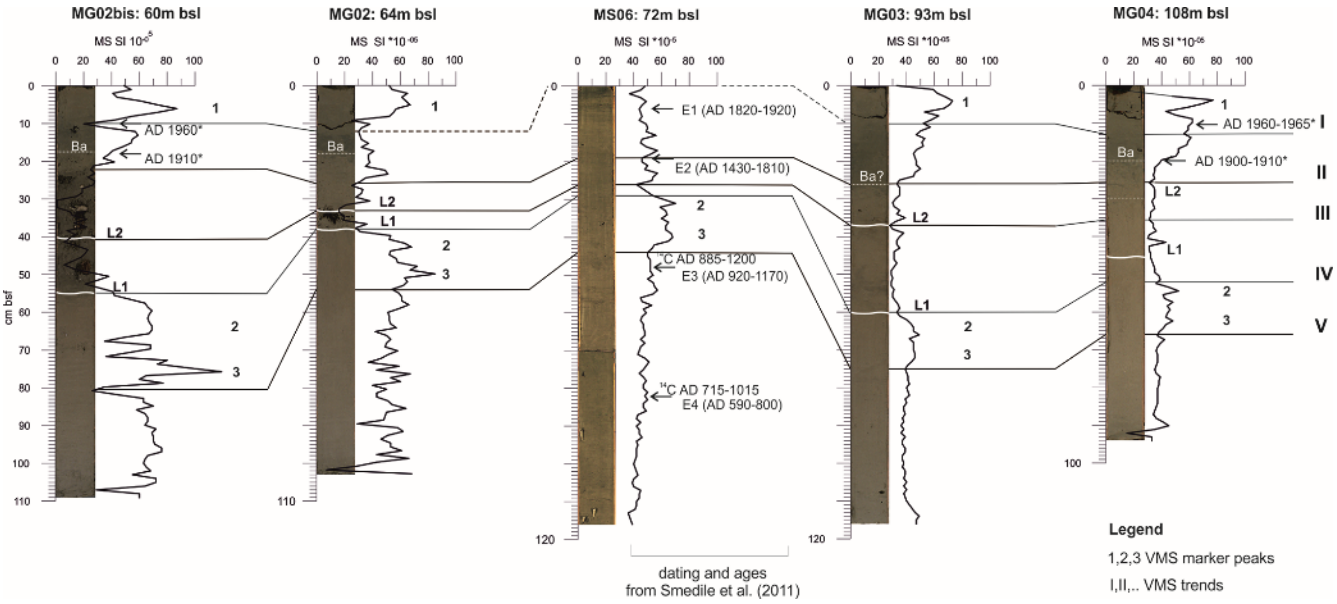

Figure 8 – Photos of cores MG displaying only the bottom limit of the three main identified units (L1, L2 and Bh), MS06 core photo of the uppermost 116 cm and relative VMS plots. Cores are organized following their depth distribution along the shelf. In core MS06 already published ^{14}C calibrated ages and modelled ages obtained for the three uppermost backwash tsunami signatures are also shown. Ages with asterisks are derived from ^{210}Pb chronology. VMS correlations are based on the five highlighted increasing /decreasing VMS trends (labelled with roman numbers at the right side of the picture) as well as on the three recognized VMS marker peaks (numbers next to each VMS peak). Such correlation allowed us to transfer ^{14}C dating, carried out on core MS06 (Smedile *et al.*, 2011) to MG cores. Note how the VMS trends III and IV followed the L1 and L2 base limits and matched with the E2 event found in core MS06.

VMS trends indicate that the L1 and L2 units, whose upper and lower limits are roughly marked by VMS trends II and IV (Fig. 8), correspond with a MS06 depth interval of 19-29 cm bsf. The uppermost limit of this latter interval is also marked by the occurrence of event E2 in MS06. Moreover, one more correlation can be found among the five cores as highlighted by the VMS minima (trend III) that marked the L2 erosional feature, apart for core MG04 where L2 limit is not clearly highlighted.

In core MS06 the E2 event, highlighted by an important sandy component increment and displaced epiphytic foraminifera (with *N. lucifuga* the most abundant taxa), was assigned to the AD 1693 tsunami although a larger age interval was modelled (AD 1430-1810). This is based on the fact that the AD 1693 event (M_{aw}=7.4) represents the strongest tsunami for this area in the modelled age interval (Maramai *et al.*, 2014) as also recorded in historical reports: "at Augusta and Siracusa after the first withdrawal and inundation second extraordinary withdrawal was observed: the sea withdrew for about 25-30 paces and then the sea level rose for more than 8 feet respect to its usual level" (Boccone, 1697). Even if for the AD 1693 event two main waves were described, which might correspond to L1 and L2, the reduced thickness of L1 unit and its lack of continuity with the uppermost L2 unit, as shown in core MG03, suggest that another tsunami might have occurred in the same area around that time.

Actually the recently updated historical seismic catalogue CFTI5Med (Guidoboni *et al.*, 2018) reports one more tsunami that occurred in AD 1542. This last event, classified as due to a local earthquake, was located in south-east Sicily, with a M_{aw}=6.4, reporting tsunami evidence only for the study area where: "after the earthquake the sea flooded the town of Augusta" (Lacisio, 1543). It is noteworthy that the AD 1542 tsunami, being close in time and location to the AD 1693 regional event, could be easily overprinted both in terms of sedimentary features and ages. In fact, onshore tsunami studies reported in Augusta Bay only found evidence for one event (PR-01 of De Martini *et al.*, 2011) in the time interval including both AD 1542 and AD 1693 but considered more likely related to the larger AD 1693 tsunami. Following this work, we cannot certainly endorse L1 as related to the AD 1542 and L2 to the AD 1693 tsunami backwash because of the absence of a clear regular boundary separating the two units. Nevertheless, as the AD 1693 event was larger and considering the marked erosive surface of L2 shown in MG02bis and MG02 cores, it is possible to infer that L1 and L2 are linked to two distinct tsunamis. Moreover, it is not possible to exclude that the E2 event in the MS06 core might be thicker taking into

account different sampling spacing adopted for MS06 with respect to cores MG and more conservative core collection procedure and tools used in this last cruise.

Finally, despite the detailed performed analyses, no further reliable matches among the discussed results can be traced in the MG cores to refer to E1 and E3 events of core MS06. Evidence for the AD 1908 tsunami that was found in core MS06 was absent in cores MG. Hence, it is only possible to speculate that the organic-rich Bh layer, dated AD 1900-1910, could be linked to that tsunami. However, the ^{210}Pb profiles recognized two phases of increases in deposition rate at the topmost limit of the Bh layer that may easily be linked to port development at Augusta, whose major harbor sea walls were completed in the early 1960s (Romano *et al.*, 2016).

CONCLUSIONS

Offshore of Augusta Bay, four sediments cores collected along an almost E-W transect from 60 to 110 m bsl, revealed the preserved remains of at least two high energy events likely associated to two tsunamis that occurred in AD 1542 and AD 1693. Those events exhibited evidence compatible with backwash tsunami signatures previously identified in Augusta Bay (MS06 core) as well as in 2004 Indian Ocean and 2011 Tohoku-oki tsunami deposits. A younger anomalous horizon (Bh layer) does not fit properly the criteria of tsunami-laid sediments listed above, but might correspond with the AD 1908 tsunami.

Amongst all the techniques applied, sedimentology and displaced benthic foraminifera remained the most informative, reinforced by the XRF results. The compared study of multiple cores collected at different depths along the shelf provided important insights about the dynamics of tsunami backwash and its imprint in the offshore stratigraphic sequence not easily gained from a single core. This work verified also the strong textural signature (sand-sized unit) to the morpho-bathymetry arrangement

related to the core position and that different procedures in core sampling (piston vs gravity coring) can affect the stratigraphy of retrieved sequences.

In conclusion, this work adds to previous ones in highlighting the growing potential of offshore investigations for reconstructing paleotsunami histories of critical relevance to test tsunami hazard models and scenarios.

ACKNOWLEDGEMENTS

The research leading to these results has received funding from the European Union's Seventh Framework Programme (FP7/2007-2013) under grant agreement n◦ 603839 (Project ASTARTE - Assessment, Strategy and Risk Reduction for Tsunamis in Europe). C. Carmisciano (INGV) and Cdr. M. Demarte (Italian Navy) are acknowledged for the technical assistance in planning coring operation. We kindly thank the Captain, the officers and the crew of the Magnaghi for their skilled technical assistance during the cruise operations. Short lived radionuclides measurements were acquired thanks to an INGV-IRSN research agreement and S. Beize, S. Bassot E. Barker are kindly acknowledged. M Nazzari is thanked for the assistance of SEM pictures performed at INGV–Roma. Many thanks to L. Pizzimenti for editing of Figure 1. We are indebted with S. Barbano (University of Catania) that helped us for the logistic of the sampling of MG cores. We wish to thank the three anonymous reviewers and the Associated Editor Pedro Costa whose suggestions contributed to substantially improve the original manuscript.

REFERENCES

Abrantes, F., Alt-Epping, U., Lebreiro, S., Voelker, A. and Schneider, R. (2008) Sedimentological record of tsunamis on shallow-shelf areas: the case of the 1969 AD and 1755 AD tsunamis on the Portuguese Shelf off Lisbon. *Mar. Geol.,* **249**, 283–293.

Appleby, P.G. (2001) Chronostratigraphic techniques in recent sediments. In: *Tracking environmental change using lake sediments volume 1: basin analysis, coring, and chronological techniques* (Eds Last, W.M. and Smol, J.P.). Kluwer Academic, 171—203.

Barbano, M.S., Pirrotta, C. and Gerardi, F. (2010) Large boulders along the south-eastern Ionian coast of Sicily: storm or tsunami deposits? *Mar. Geol.,* **275** (1-4), 140-154. https://doi.org/10.1016/j.margeo.2010.05.005

Bellucci, L.G., Giuliani, S., Romano S., Albertazzi, S., Mugnai, C. and Frignani, M. (2012) An Integrated Approach to the Assessment of Pollutant Delivery Chronologies to Impacted Areas: Hg in the Augusta Bay (Italy). *Environ. Sci. Technol*., **46,** 2040−2046. dx.doi.org/10.1021/es203054c

Bergamin, L. and Romano, E. (2016) Suitable sediment fraction for paleoenvironmental reconstruction and assessment of contaminated coastal areas based on benthic foraminifera: A case study from Augusta Harbour (Eastern Sicily, Italy). *Ecological Indicators,* **71**, 66–78. http://dx.doi.org/10.1016/j.ecolind.2016.06.030

Boccone, P. (1697*) Intorno il terremoto della Sicilia seguito l'anno 1693.* Museo di Fisica, Venezia.

Budillon, F., Ferraro, L., Hopkins, T.S., Iorio, M., Lubritto, C., Sprovieri, M., Bellonia, A., Marzaioli, F. and Tonielli, R. (2008). Effects of intense anthropic settlement of coastal areas on sea-bed and

sedimentary systems: a case study from the Augusta Bay (Southern Italy). *Rendiconti online della Società Geologica Italiana*, **3**, 142–143.

Chagué-Goff, C., Chan, J.C.H., Goff, J. and Gadd, P. (2016) Late Holocene record of environmental changes, cyclones and tsunamis in a coastal lake, Mangaia, Cook Islands. *Island Arc*, **25**, 333–349.

Chagué-Goff, C., Schneider, J.-L., Goff, J.R., Dominey-Howes, D. and Strotz, L. (2011) Expanding the proxy toolkit to help identify past events - lessons from the 2004 Indian Ocean tsunami and the 2009 South Pacific tsunami. *Earth Sci. Rev*., **107**, 107–122.

Chagué-Goff, C., Szczuciński, W. and Shinozaki, T. (2017) Applications of geochemistry in tsunami research: A review. *Earth Sci. Rev*., **165**, 203-244.

Cimerman, F. and Langer, M.R. (1991) *Mediterranean Foraminifera*. Academia Scientiarum et Artium Slovenica Classis IV 30, Ljubljana, 118 pp.

Collins, P.E.F., Turner, S.D. and Cundy, A.B. (2001) High-resolution reconstruction of recent vegetation dynamics in a Mediterranean microtidal wetland: implications for site sensitivity and palaeoenvironmental research. *J. Coastal Res.,* **17** (3), 684-693.

Croudace I.W., Romano E., Ausili A., Bergamin L. and Rothwell G. (2015) X-ray core scanners as an environmental forensics tool: a case study of polluted harbour sediment (Augusta Bay, Sicily). In: *Micro-XRF Studies of Sediment Cores* (Eds Croudace I.W., Rothwell G.), chapter 15, Springer Developments in Environmental Research (Series Editor - J.P. Smol). Springer, Berlin.

Cundy, A.B. and Croudace, I.W. (1996) Sediment Accretion and Recent Sea-level Rise in the Solent, Southern England: Inferences from Radiometric and Geochemical Studies. *Estuar., Coastal and Shelf Sci.*, **43**(4), 449-467. DOI: 10.1006/ecss.1996.0081

Cundy, A.B, Collins, P.E.F., Turner, S.D., Croudace, I.W. and Horne, D. (1998) 100 years of environmental change in a coastal wetland, Augusta Bay, southeast Sicily: evidence from geochemical and palaeoecological studies. In: *Sedimentary Processes in the Intertidal Zone Black* (Eds K.S., Paterson, D.M., Cramp, A.). Geological Society, London, Special Publication, **139**, 243–254.

Dawson, A.G. and Stewart, I. (2007) Tsunami deposits in the geological record. *Sediment. Geol*., **200**, 166–183.

Decembrini, F., Hopkins, T.S. and Azzaro, F. (2004) Variability and sustenance of the deep chlorophyll maximum over a narrow shelf, Augusta Gulf (Sicily). *Chemistry and Ecology*, **20** (1), 231–247.

De Martini, P.M., Barbano, M.S., Smedile, A., Gerardi, F., Pantosti, D., Del Carlo, P. and Pirrotta, C. (2010) A unique 4000 year long geological record of multiple tsunami inundations in the Augusta bay (eastern Sicily, Italy). *Mar. Geol*., **276**, 42–57. http://dx.doi.org/10.1016/j.margeo.2010.07.005.

De Martini, P.M., Barbano, M.S., Pantosti, D., Smedile, A., Pirrotta, C., Del Carlo, P. and Pinzi, S. (2012) Geological evidence for paleotsunami along eastern Sicily (Italy): an overview. *Nat. Hazards Earth Syst. Sci.,* **12**, 2569-2580. DOI: 10.5194/nhess-12-2569-2012.

Di Leonardo, R., Bellanca, A., Capotondi. A., Cundy, A. and Neri, R. (2007) Possible impacts of Hg and PAH contamination on benthic foraminiferal assemblages: An example from the Sicilian coast, central Mediterranenan. *Sci. Total Environ.,* **338**, 168-183.

Di Leonardo, R., Bellanca, A., Angelone, M., Leopardi, M. and Neri, R. (2008) Impact of human activities on the central Mediterranean offshore: Evidence from Hg distribution in box-core sediments from the Ionian. *Sea. Appl. Geochem*., **23**, 3756−3766.

Di Leonardo, R., Bellanca, A., Neri, R., Tranchida, G. and Mazzola, S. (2009) Distribution of REEs in box-core sediments offshore an industrial area in SE Sicily, Ionian Sea: Evidence of anomalous sedimentary inputs. *Chemosphere*, **77**, 778-784.

Di Leonardo, R., Mazzola, S., Cundy, A.B., Tramati, C.D. and Vizzini, S (2017) Trace element storage capacity of sediments in dead *Posidonia oceanica* mat from a chronically contaminated marine ecosystem. *Environmental Toxicology and Chemistry*, **36** (1), 49–58.

Droser, M.J. and Bottjer, D.J. (1991) Trace fossils and ichnofabric in Leg 119 cores. *Proceedings ODP. Sci. Result*, **119**, 635-641.

Feldens, P., Schwarzer, K., Sakuna, D., Szczuciński, W. and Somgpongchaiykul, P. (2012) Sediment distribution on the inner continental shelf off Khao Lak (Thailand) after the 2004 Indian Ocean Tsunami. *Earth Planets Space,* **64**, 875–887.

Fiorini, F. and Vaiani, S.C. (2001) Benthic foraminifers and transgressive–regressive cycles in the Late Quaternary subsurface sediments of the Po Plain near Ravenna (Northern Italy). *Bollettino della Società Paleontologica Italiana*, **40**, 357–403.

Firetto Carlino, M., Di Stefano, A. and Budillon F. (2013) Seismic facies and seabed morphology in a tectonically controlled continental shelf: The Augusta Bay (offshore eastern Sicily, Ionian Sea). *Mar. Geol.*, **335**, 35-51.

Goff, J., Chagué-Goff, C., Nichol, S., Jaffe, B. and Dominey-Howes, D. (2012) Progress in palaeotsunami research. *Sediment. Geol.*, **243–244**, 70–88.

Goldberg E.D. (1963) Geochronology with ^{210}Pb in radioactive dating. IAEA, Vienna 121-131.

Goodman-Tchernov, B.N., Dey, H.W., Reinhardt, E.G., McCoy, F. and Mart, Y. (2009) Tsunami waves generated by the Santorini eruption reached eastern Mediterranean shores. *Geology*, **37**, 943–946. http://dx.doi.org/10.1130/G25704A.1.

Goodman Tchernov, B., Katz, T., Shaked, Y., Qupty, N., Kanari, M., Niemi, T., Agnon, A. (2016) Offshore Evidence for an Undocumented Tsunami Event in the 'Low Risk' Gulf of Aqaba-Eilat, Northern Red Sea. *PLoS One*, **11**, e0145802. doi:10.1371/journal.pone.0145802

Grasso, M. and Lentini, F. (1982) Sedimentary and tectonic evolution of the eastern Hyblean Plateau (southeastern Sicily) during late Cretaceous to Quaternary time. *Palaeogeogr. Palaeoclimatol. Palaeoecol.,* **39**, 261-280.

Guidoboni, E., Ferrari, G., Mariotti, D., Comastri, A., Tarabusi, G., Sgattoni, G. and Valensise G. (2018) *CFTI5Med, Catalogo dei Forti Terremoti in Italia (461 a.C.-1997) e nell'area Mediterranea (760 a.C.-1500).* Istituto Nazionale di Geofisica e Vulcanologia (INGV). http://storing.ingv.it/cfti/cfti5/

Hammer, Ø., Harper, D.A.T. and Ryan, P.D. (2001) PAST: Paleontological Statistics Software Package for Education and Data Analysis. *Palaeontologia Electronica*, **4**(1), 9pp. http://palaeo-electronica.org/2001_1/past/issue1_01.htm

Haug, G.H., Hughen, K.A., Sigman, D.M., Peterson, L.C. and Rohl, U. (2001) Southward migration of the intertropical convergence zone through the Holocene. *Science* **293**(5533), 1304-1308.

Ikehara, K., Irino, T., Usami, K., Jenkins, R., Omurad, A. and Ashi, J. (2014) Possible submarine tsunami deposits on the outer shelf of Sendai Bay, Japan resulting from the 2011 earthquake and tsunami off the Pacific coast of Tohoku. *Mar. Geol.*, **358**, 120–127.

ISPRA (2011) Note illustrative della Carta Geologica d'Italia scala 1:50 000, Foglio 641 Augusta, 2011, p. 248.

Lacisio, P. (1543) Lettera di Paolo Lacisio ad Amerbach, Strasburgo 7 marzo 1543. In: Hartmann, A. (Ed.), *Die Amerbachkorrespondens*, **5**, Basel 1858, 414 pp.

Langer, M.R. (1993) Epiphytic foraminifera. *Mar. Micropal*., **20**, 235–265.

Loeblich, R. and Tappan, H. (1987) *Foraminiferal genera and their classification*. Van Nostrand Reinhold, New York.

Löwemark, L., Chen, H.F., Yang, T.N., Kylander, M., Yu, E.F., Hsu, Y.W., Lee, T.Q.S., Song, R. and Jarvis S. (2011) Normalizing XRF-scanner data: a cautionary note on the interpretation of high-resolution records from organic-rich lakes. *J. Asian Earth Sci.*, **40**, 1250-1256.

Lisi, A. Taramelli, M. Di Risio, S. Cappucci and Gabellini, M. (2009) Flushing efficiency of Augusta Harbour (Italy). *J. Coast. Res.,* **56**, 841-845.

Jonathan, M.P., Srinivasalu, S., Thangadurai, N., Rajeshwara-Rao, N., Ram-Mohan, V. and Narmatha, T. (2012) Offshore depositional sequence of 2004 tsunami from Chennai, SE coast of India. *Nat. Hazards*, **62**, 1155–1168.

Jorissen, F.J. (1987). The distribution of benthic Foraminifera in the Adriatic Sea. *Marine Micropaleontology*, **12**, 21-48.

Kortekaas, S. and Dawson, A.G. (2007) Distinguishing tsunami and storm deposits: an example from Martinhal, SW Portugal. *Sediment. Geol.,* **200** (3-4), 208-221.

Magagnoli, A. and Mengoli, M. (2000) Un brevetto CNR per la campionatura dei fondali marini. In: E.Bonatti, L.Gasperini, M.Ligi, M. Ravaioli (Eds.), "I due terzi oscuri del nostro Pianeta: la geologia della Terra sommersa". *Ricerca & Futuro*, **14**, 67-68.

Mamo, B., Strotz, L. and Dominey-Howes, D. (2009) Tsunami sediments and their foraminiferal assemblages. *Earth Sci. Rev*., **96**, 263-278.

Maramai A., Brizuela B. and Graziani L. (2014) The Euro-Mediterranean Tsunami Catalogue, *Annals of Geophysics,* **57** (4).

Mateu-Vicens, G., Brandano, M., Gaglianone, G. and Baldassarre A. (2012) Seagrass-meadow sedimentary facies in a mixed siliciclasticcarbonate temperate system in the Tyrrhenian Sea (Pontinian Islands, western Mediterranean). *J. Sediment. Res*., **82**,451–463

Mateu-Vicens, G., Khokhlova, A. and Sebastián-Pastor, T (2014) Epiphytic foraminiferal indices as bioindicators in Mediterranean seagrass meadows. *J. Foramin. Res.*, **44**,325–339

Milker, Y., Wilken, M., Schumann, J., Sakuna, D., Feldens, P., Schwarzer, K. and Schmiedl, G. (2013) Sediment transport on the inner shelf off Khao Lak (Andaman Sea, Thailand) during the 2004 Indian Ocean tsunami and former storm events: evidence from foraminiferal transfer functions. *Nat. Hazards Earth Syst. Sci.,* **13**, 3113–3128. http://dx.doi.org/10.5194/nhess-13-3113-2013.

Morton, R.A., Gelfenbaum, G. and Jaffe, B.E. (2007) Physical criteria for distinguishing sandy tsunami and storm deposits using modern examples. *Sediment. Geol.,* **200**, 184-207.

Murray, J.W. (2006) *Ecology and applications of Benthic Foraminifera*. Cambridge University Press, Cambridge.

Paris, R., Fournier, J., Poizot, E., Etienne, S., Morin, J., Lavigne, F. and Wassmer, P. (2010) Boulder and fine sediment transport and deposition by the 2004 tsunami in Lhok Nga (western Banda Aceh, Sumatra, Indonesia): a coupled offshore-onshore model. *Mar. Geol.*, **268**, 43–54. http://dx.doi.org/10.1016/j.margeo.2009.10.011.

Parker, W.C. and Arnold, A.J. (1999) Quantitative methods of data analysis in foraminiferal ecology. In: *Modern Foraminifera* (Ed Sen Gupta, B.K.). Kluver Academic Publisher, London, 71-89.

Pilarczyk, J.E. and Reinhardt, E.G. (2012) *Homotrema rubrum* (Lamarck) taphonomy as in overwash indicator in Marine Ponds on Anegada, British Virgin Islands. *Natural Hazards*, **63**, 85–100.

Pilarczyk, J.E., Horton, B.P., Witter, R.C., Vane, C.H., Chagué-Goff, C., Goff, J. (2012) Sedimentary and foraminiferal evidence of the 2011 Tōhoku-oki tsunami on the Sendai coastal plain, Japan. *Sediment. Geol.,* **282**, 78–89. doi:10.1016/j.sedgeo.2012.08.011

Pilarczyk, J.E., Dura, T., Horton, B.P., Engelhart, S.E., Kemp, A.C. and Sawai, Y. (2014) Microfossils from coastal environments as indicators of paleo-earthquakes, tsunamis and storms. *Palaeogeogr. Palaeoclimatol. Palaeoecol.,* **413**, 144–157.

Pirrotta, C., Barbano, M.S., Pantosti, D. and De Martini, P.M. (2013) Evidence of active tectonics in the Augusta Basin (eastern Sicily, Italy) by Chirp sub-bottom sonar investigation. *Annals of Geophysics,* **56** (5). doi:10.4401/ag-6371

Quintela, M., Costa, P.J.M., Fatela, F., Drago, T., Hoska, N., Andrade, C. and Freitas, M.C. (2016) The AD 1755 tsunami deposits onshore and offshore of Algarve (south Portugal): sediment transport interpretations based on the study of foraminifera assemblages. *Quat. Int.,* **408**, 123–138.

Raffa, F. and Hopkins, T.S. (2004) Circulation and water mass structure over a narrow shelf, Augusta Gulf (Sicily). *Chemistry and Ecology*, **20**(1), 249–266.

Reimer, P.J., Bard, E., Bayliss, A., Beck, J.W., Blackwell, P.G., Bronk Ramsey, C., Grootes, P.M., Guilderson, T.P., Haflidason, H., Hajdas, I., Hatte, C., Heaton, T.J., Hoffmann, D.L., Hogg, A.G., Hughen, K.A., Kaiser, K.F., Kromer, B., Manning, S.W., Niu, M., Reimer, R.W., Richards, D.A., Scott, E.M., Southon, J.R., Staff, R.A., Turney, C.S.M. and van der Plicht, J. (2013) IntCal13 and Marine13 radiocarbon age calibration curves 0e50,000 Years cal BP. *Radiocarbon,* **55**, 1869-1887.

Rhodes, B., Tuttle, M., Horton, B., Doner, L., Kelsey, H., Nelson, A. and Cisternas, M. (2006) Paleotsunami Research. *Eos*, Trans. Am. Geophys. Union 87, 205–209.

Romano, E., Bergamin, L., Finoia, M.G., Celia Magno, M., Ausili, A. and Gabellini, M. (2009) The effects of human impact on benthic foraminifera in the Augusta Harbour (Sicily, Italy). In: *Proceedings of the International Symposium on Integrated Coastal Zone Management* (Eds Dahl E, Moksness E, Støttrup J), Wiley-Blackwell, Chichester, p 97-115

Romano, E., Bergamin, L., Celia Magno, M. and Ausili, A. (2013) Sediment characterization of the highly impacted Augusta Harbour (Sicily, Italy): modern benthic foraminifera in relation to grain-size and sediment geochemistry. Environ Sci: *Processes Impacts,* **15**, 930–946

Romano E., Bergamin L., Ausili A., Celia Magno M. and Gabellini M. (2015) Evolution of the anthropogenic impact in the Augusta Harbor (Eastern Sicily, Italy) in the last decades: Benthic foraminifera as indicators of environmental status. *Environ. Sci. Pollut. Res*. DOI 10.1007/s11356-015-5783-x

Romano E., **Bergamin L., Ausili A., Celia Magno M. and Gabellini M. and Croudace I.W.** (2018) Differences in acquisition of environmental data in strongly impacted marine sediments using gravity and vibro corers: The case-study of Augusta harbor (Eastern Sicily, Italy). *Measurement*, **124**, 184-190.

Sagnotti, L., Smedile, A., De Martini, P.M., Pantosti, D., Speranza, F., Winkler., A., Del Carlo, P., Bellucci, L.G. and Gasperini, L. (2011) A continuous palaeosecular variation record of the last four millennia from the Augusta Bay (Sicily, Italy). Geophys. *J. Int.,* **184**, 191-202.

Sakuna, D., Szczuciński, W., Feldens, P., Schwarzer, K. and Khokiattiwong, S. (2012) Sedimentary deposits left by the 2004 Indian Ocean tsunami on the inner continental shelf offshore of Khao Lak, Andaman Sea (Thailand). *Earth Planets Space*, **64**, 931–943.

Scicchitano, G., Monaco, C. and Tortorici, L. (2007) Large boulder deposits by tsunami waves along the Ionian coast of south-eastern Sicily (Italy). *Mar. Geol.*, **238**, 75–91.

Scicchitano, G., Costa, B., Di Stefano, A., Longhitano, S. G. and Monaco, C. (2010) Tsunami and storm deposits preserved within a riatype rocky coastal setting (Siracusa, SE Sicily). *Z. Geomorphol.*, **54**, Suppl. 3, 51–77.

Scott, D.B., Medioli, F.S. and Schafer, C.T. (2001) *Monitoring in Coastal Environments Using Foraminifera and Thecamoebian Indicators*. Cambridge University Press, Cambridge.

Seike, K., Shirai, K. and Kogure, Y. (2013) Disturbance of shallow marine soft-bottom environments and megabenthos assemblages by a huge tsunami induced by the 2011 M9.0 Tohoku-Oki earthquake. *PloS One*, **8**, e65417.

Seike, K., Kitahashi, T. and Noguchi, T. (2016) Sedimentary features of Onagawa Bay, northeastern Japan after the 2011 off the Pacific coast of Tohoku Earthquake: sediment mixing by recolonized benthic animals decreases the preservation potential of tsunami deposits. *J. Ocean.*, **72**, 141–149.

Seike, K., Kobayashi, G. and Kogure, K. (2017) Post-depositional alteration of shallow-marine tsunami-induced sand layers: A comparison of recent and ancient tsunami deposits, Onagawa Bay, northeastern Japan. *Island Arc,.* **26**, e12174. https://doi:10.1111/iar.12174

Sen Gupta, B. K. (1999) Systematics of modern foraminifera. In: *Modern Foraminifera* (Ed. Sen Gupta, B.K.). Kluwer Academic Publishers, London, 7–36.

Sgarrella, F. and Moncharmont Zei, M. (1993) Benthic foraminifera of the Gulf of Naples (Italy): systematics and autoecology. *Bollettino della Società Paleontologica Italiana*, **32**, 145–264.

Shanmugam, G. (2012) Process-sedimentological challenges in distinguishing paleo-tsunami deposits. *Nat. Hazards,* 63**,** 5–30. http://dx.doi.org/10.1007/s11069-011-9766-z.

Shiki, T., Tachibana, T., Fujiwara, O., Goto, K., Nanayama, F. and Yamazaki, T. (2008) Characteristic features of tsunamiites. In: *Tsunamiites - Features and Implications* (Eds Shiki, T., Tsuji, Y., Yamazaki, T., Minoura, K.). Elsevier, Amsterdam, pp. 319-340.

Shinozaki, T., Goto, K., Fujino, S., Sugawara, D. and Chiba, T. (2015) Erosion of a paleo-tsunami record by the 2011 Tohoku-oki tsunami along the southern Sendai Plain. *Mar. Geol.*, **369**, 127–136.

Smedile, A., De Martini, P. M., Pantosti, D., Bellucci, L.G., Del Carlo, P., Gasperini, L., Pirrotta, C., Polonia, A., and Boschi, E. (2011) Possible tsunami signatures from an integrated study in the Augusta Bay offshore (Eastern Sicily-Italy). *Mar. Geol.*, **281**, 1–13.

Smedile, A., De Martini, P.M. and Pantosti, D. (2012) Combining inland and offshore paleotsunamis evidence: The Augusta Bay (eastern Sicily, Italy) case study. *Nat. Hazards Earth Syst. Sci.,* **12**, 2557-2567.

Sprovieri, M., Oliveri, E., Di Leonardo, R., Romano, E., Ausili, A., Gabellini, M., Barra, M., Tranchida, G., Bellanca, A., Neri, R., Budillon, F., Saggiomo, R., Mazzola, S. and Saggiomo, V. (2011) The key role played by the Augusta basin (southern Italy) in the mercury contamination of the Mediterranean Sea. *J. Environ. Monit.*, **13**, 1753–1760.

Stuut, J.-B.W., Kasten, S., Lamy, F., and Hebbeln, D. (2007) Sources and modes of terrigenous sediment input to the Chilean continental slope. *Quatern. Intern.,* **161**(1), 67-76.

Sugawara, D., Minoura, K., Nemoto, N., Tsukawaki, S., Goto, K. and Imamura, F. (2009) Foraminiferal evidence of submarine sediment transport and deposition by backwash during the 2004 Indian Ocean tsunami). *Island Arc*, **18**, 513–525.

Tamura, T., Sawai, Y., Ikehara, K., Nakashima, R., Hara, J. and Kanai, Y. (2015) Shallow marine deposits associated with the 2011 Tohoku-oki tsunami in Sendai Bay, Japan. *Journal of Quaternary Science*, **30,** 293-297.

Toyofuku, T., Duros, P., Fontanier, C., Mamo, B., Bichon, S., Buscail, R., Chabaud, G., Deflandre, B., Goubet, S., Grémare, A., Menniti, C., Fujii, M., Kawamura, K., Koho, K.A., Noda, A., Namegaya, Y., Oguri, K., Radakovitch, O., Murayama, M., de Nooijer, L.J., Kurasawa, A., Ohkawara, N., Okutani, T., Sakaguchi, A., Jorissen, F., Reichart, G.J. and Kitazato, H. (2014) Unexpected biotic resilience on the Japanese seafloor caused by the 2011 Tōhoku-Oki tsunami. *Sci. Rep.*, **4:7517**. http://dx.doi.org/10.1038/srep07517.

Tyuleneva, N., Braun, Y., Suchkov, I., Katz, T., Ben-Avraham, Z. and Goodman-Tchernov, B. (2018) A new chalcolithic-era tsunami event identified in the offshore sedimentary record of Jisr al-Zarka (Israel). *Mar. Geol.* http://dx.doi.org/10.1016/j.margeo.2017.07.008

Van der Zwaan, G.J., Jorissen, F.J. and de Stigter, H.C. (1990) The depth dependency of planktonic/ benthic foraminiferal ratios: constraints and applications. *Mar. Geol*., **95**, 1–16.

Yarincik, K.M., Murray, R.W. and Peterson, L.C. (2000) Climatically sensitive eolian and hemipelagic deposition in the Cariaco Basin, Venezuela, over the past 578,000 years: results from Al/Ti and K/Al. *Paleocean.* **15**,210–228.

Yoshikawa, S., Kanamatsu, T., Goto, K., Sakamoto, I., Yagi, M., Fujimaki, M., Imura, R., Nemoto, K. and Sakaguchi, H. (2015) Evidence for erosion and deposition by the 2011 Tohoku-oki tsunami on the nearshore shelf of Sendai Bay, Japan. *Geo-Mar Lett.* DOI 10.1007/s00367-015-0409-3.

Wang, Q.D., Song, J.M., Li, X.G.; Yuan, H.M., Li, N., Cao, L. (2015) Environmental radionuclides in a coastal wetland of the Southern Laizhou Bay, China*. Marine Pollution Bulletin*, **97**, 506-511.

Weiss, R. and Bahlburg, H. (2006) A note on the preservation of offshore tsunami deposits. *J. Sediment. Res.*, **76**, 1267–1273. http://dx.doi.org/10.2110/jsr.2006.110.